DEFORMATION CHARACTERISTICS

OF W-Zn COMPOSITES

by

SATHISH RAO BALA

B.Sc., University of Mysore, INDIA, (1965).
B.E., Indian Institute of Science, Bangalore, INDIA, (1969).

A THESIS SUBMITTED IN PARTIAL FULFILMENT OF

THE REQUIREMENTS FOR THE DEGREE OF

MASTER OF APPLIED SCIENCE

in the Department

of

Metallurgy

We accept this thesis as conforming to the
required standard

THE UNIVERSITY OF BRITISH COLUMBIA

December, 1971

In presenting this thesis in partial fulfilment of the requirements for an advanced degree at the University of British Columbia, I agree that the Library shall make it freely available for reference and study. I further agree that permission for extensive copying of this thesis for scholarly purposes may be granted by the Head of my Department or by his representatives. It is understood that copying or publication of this thesis for financial gain shall not be allowed without my written permission.

Department of   Metallurgy

The University of British Columbia
Vancouver 8, Canada

Date   December 17, 1971

A B S T R A C T

The deformation characteristics of continuous tungsten fibre-reinforced zinc composites have been investigated. Composites with a single crystal matrix containing up to 4.5 volume per cent of tungsten fibres were studied.

The stress-strain curves of W-Zn composites showed positive deviations from the "rule of mixture" predictions. Theoretical work attributes the positive deviations to matrix hardening due to either one of the phenomena:

(a) the difference in the lateral contractions of the fibre and the matrix;

(b) the pile up of dislocations in the matrix at the matrix-fibre interface.

In the present work the positive deviations in the elastic-plastic region of the stress-strain curves of the composites have been attributed to both (a) and (b).

The positive deviations in the ultimate tensile strengths of the composites have been attributed to (b).

Composites containing up to 0.08 volume per cent of the tungsten wires deformed even after the fracture of the fibres. Dissolution of the matrix of these deformed composites showed that multiple necking had occurred in the fibres fractured to 1-5 mms length.

Composites containing greater than 0.08 volume per cent of tungsten fibres fractured by cleaving through the basal plane of the matrix.

No fibre fracture inside the matrix was seen except at the fracture end of the composite. Multiple necking of the fibres near the fractured end has been seen only in those composites which have deformed more than the free fibres tested individually.

ACKNOWLEDGEMENT

TABLE OF CONTENTS

LIST OF FIGURES

LIST OF TABLES

I. INTRODUCTION

A. General:

In recent years much attention has been given to the possibility of increasing the strength of weaker materials by reinforcing them with stronger materials. Very good strength characteristics are found in materials which contain a large volume fraction of a hard second phase uniformly distributed through the major phase. These types of materials can be obtained by phase decomposition, by mechanical mixing and sintering (powder metallurgical means), and by internal oxidation.

The strength properties of these materials entirely depend on the properties of the hard phase present in the weak matrix. Investigations on these materials led to the conclusion that a matrix containing uniformly dispersed needle shaped hard particles, with a good bonding of the harder phase to the matrix, would give maximum strength.

Recent investigators have considered combinations of strong fibrous materials with relatively weak binder materials in order to obtain strong composites. This has led to the fabrication of composite materials with mechanical properties superior to those of the bulk materials from which they are derived. Various techniques have been developed for incorporating strong fibres in the weaker matrices and many theories predicting the tensile properties have been developed.

B. Previous Work:

Much of the past research has been concerned with fabricating a good composite. Fabrication methods can be broadly classified[1] as 'direct', and 'indirect'.

Direct fabrication of fibre-reinforced metals can be carried out either by the growth and arrangement of the fibres, using a controlled phase transformation, or by production and alignment by working in the solid state. Direct fabrication is usually done in a single operation.

$CuAl_2$-Al eutectic composites,[2] Fe_2B-Fe eutectic composites,[3] Ni_3Si-Ni eutectic composites,[3] Al_3Ni-Al eutectic composites,[4] Cu-Cr eutectic composites[1] and Cu_5Ca-Cu[1] composites are some examples of composites obtained by direct fabrication methods.

The indirect method of fabrication involves two steps. The fibres are first obtained separately and are subsequently incorporated in the matrix to form the composite structure. Reinforcements have been made using either continuous or discontinuous fibres. Different approaches to the fabrication of composites, and the systems fabricated by these methods are given in Table 1.

TABLE 1. FABRICATION TECHNIQUES, AND COMPOSITE SYSTEMS FABRICATED
BY THESE TECHNIQUES

From Alexander *et al.*[5,6]

FABRICATION TECHNIQUE	FIBRE-MATRIX SYSTEM
Liquid Metal Infiltration	B-Mg, W-Cu, Mo-Cu, Ta-Cu, B-Al, W-Ni, Steel-Ag, W-Ag.

Table 1 (Continued)

FABRICATION TECHNIQUE	FIBRE-MATRIX SYSTEM
Hot Pressure Bonding	B-Al, Be-Al, Stainless Steel-Al, SiC-Al, Coated B-Al, SiO_2-Al, B-Mg, SiC-Ti, Be-Ti, B-Ti, Coated B-Ti.
Cold Press and Sinter	W-Ni, Mo-Ni, Mo-Ti, W-Ag.
Plasma Spray	B-Al, SiC-Al, Coated B-Al, W-W.
High Energy Rate Forming	B-Al, B-Ni, B-Ti, W-Al, W-Ni, SiC-Ti, SiC-Ni.
Electro-deposition	W-Ni, B-Ni, SiC-Ni, B-Al, SiC-Al, W-Cu.
Chemical Vapour Deposition	W-W, B-W, Be-Al.
Extrusion and Rolling	W-Ni, Mo-Ni, B-Al, Mo-Ti, B-Ti.

The strong fibres used in the reinforcement of a weaker matrix-binder can be divided into three groups: whiskers, metallic wires and non-metallic wires (ceramic fibres).

Composite materials can also be classified according to the fibres and matrix materials present in the composites. The different categories of composites, with examples of composite systems that have been fabricated and whose deformation characteristics have been studied, are given in Table 2.

TABLE 2. COMPOSITE GROUPS AND THE APPROPRIATE COMPOSITE SYSTEMS

FIBRE-MATRIX	COMPOSITE SYSTEM INVESTIGATED: FIBRE-MATRIX
Metal-metal	W-Ag,[7,8] W-Cu,[9,10,11] Stainless Steel-Al,[12,13,14,15] Steel-Cu,[16] Mo-Cu,[10] Ta-Cu,[17] B-Al,[18,19] etc.
Ceramic (non metal)-metal	C-Ni,[20] Al_2O_3-Ni,[21] Si_3N_4-Ag[22], SiO_2-Al,[23] Glass-Al,[24] Al_2O_3-Ti,[25] etc.
Metal-non metal	Nichrome-Al_2O_3,[26] Nichrome-SiO_2,[26] Stainless Steel - Al_2O_3,[26] Stainless Steel-SiO_2,[26] Al-plastic,[27] etc.
Non metal-non metal	Glass-plastic,[28] Carbon-polyester,[29] Si_3N_4-resin.[22]

Most extensive studies have been done on the deformation characteristics of composites containing continuous metallic fibres.

McDanels et al.[9] in their work on tungsten fibre-reinforced copper composites defined four stages of tensile deformation, Figure 1.

I.   Elastic deformation of fibre; elastic deformation of matrix.

II. Elastic deformation of fibre; plastic deformation of matrix.

III. Plastic deformation of fibre; plastic deformation of matrix.

IV. Failure of fibre and matrix.
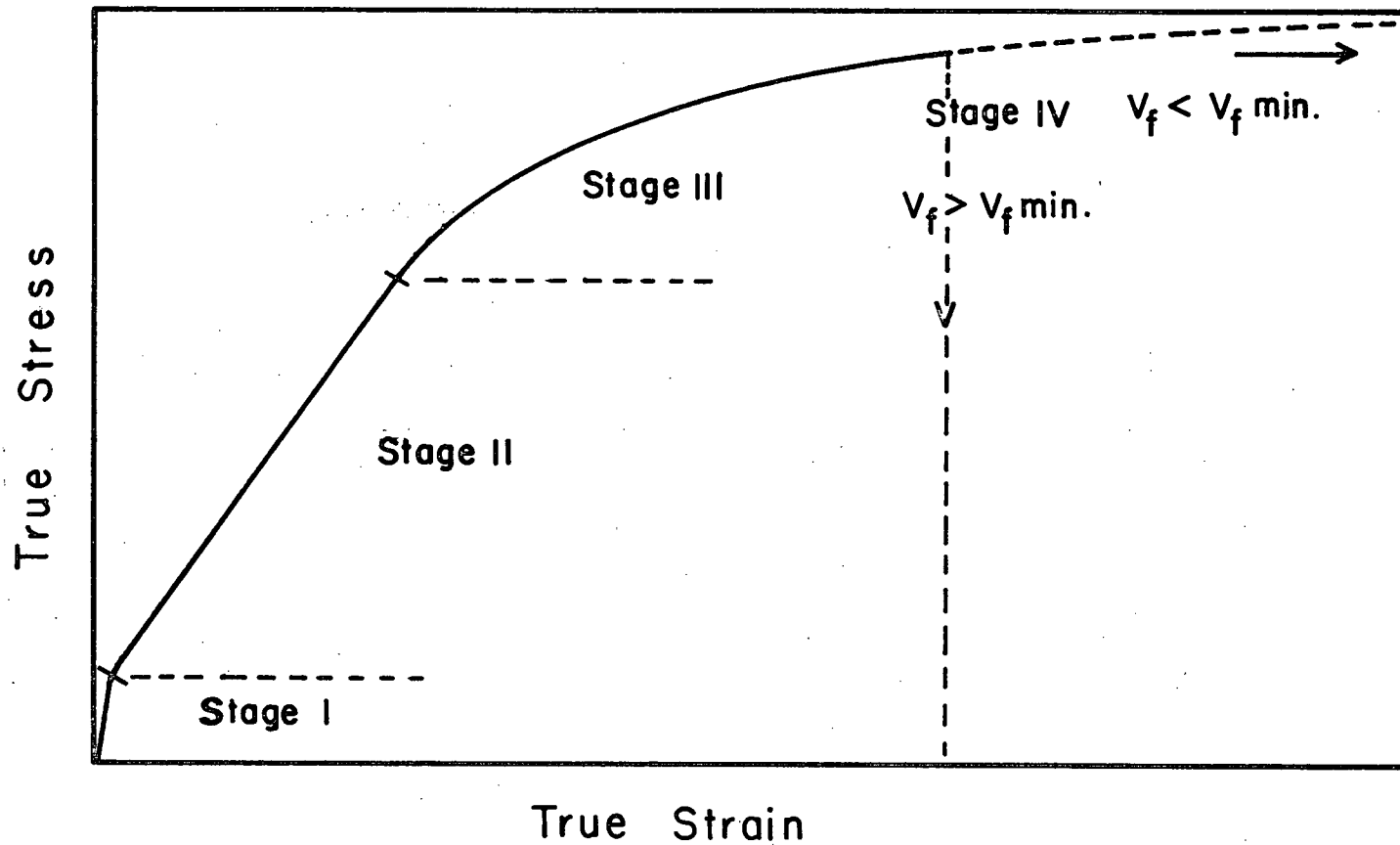
Fig. 1. Schematic Diagram of the True Stress-strain Curve of a Composite Showing Four Stages of Deformation.

The tensile properties were discussed, making use of the "rule of mixtures." The rule of mixtures is given[30] by the elementary decomposition formula:

$$\bar{f} = c_1\bar{f}_1 + c_2\bar{f}_2, \quad c_1 + c_2 = 1 \tag{1}$$

$\bar{f}$, $\bar{f}_1$ and $\bar{f}_2$ are composite, phase 1, and phase 2 averages of any function $f(x,y)$. c_1 and c_2 are phase concentrations (by volume fraction) of phases 1 and 2 respectively.

For a volume fraction of fibres greater than a certain minimum value (to be discussed later) the ultimate tensile strength of a continuous fibre composite, σ_{cu}, is given by:

$$\sigma_{cu} = \sigma_{fu}V_f + \sigma_m'V_m, \quad V_f + V_m = 1 \tag{2}$$

σ_{fu} = the ultimate tensile strength of the fibre;

σ_m' = the stress in the free matrix at the ultimate strain of the free fibre;

V_f = volume fraction of the fibre in the compsite;

V_m = volume fraction of the matrix in the composite.

Expression (2) assumes that the matrix strain ε_m, the fibre strain ε_f, and the composite strain ε_c are equal for a given load.

McDanels et al.[9] generalized equation (2) to allow prediction of the stress in a composite, σ_c, at any value of strain:

$$\sigma_c = \sigma_fV_f + \sigma_mV_m, \quad V_m + V_f = 1 \tag{3}$$

where the σ values represent stresses at any particular value of strain taken from the stress-strain curves of the components in the condition in which they exist in the composite.

On the basis of equal elastic strains in Stage I, expression (3) can be written as:

$$E_{cI} = E_f V_f + E_m V_m \qquad (4)$$

where

E_{cI} = Young's modulus of the composite in Stage I,

E_f = Young's modulus of the free fibre,

E_m = Young's modulus of the free matrix.

A similar expression was also written for Stage II of the composite stress-strain curve. Stage II was found to be linear by McDanels *et al.*[9] The slope of the second stage, $\frac{d\sigma_c}{d\varepsilon}$, or the "secondary modulus", E_{cII}, of a composite is given by:

$$E_{cII} = \frac{d\sigma_c}{d\varepsilon} = E_f V_f + \left(\frac{d\sigma_m}{d\varepsilon}\right) V_m \qquad (5)$$

where $\frac{d\sigma_m}{d\varepsilon}$ is the slope of stress-strain curve of the free matrix at a given strain. In expression (5) $E_f V_f$ is the dominating factor and hence the variation of $\left(\frac{d\sigma_m}{d\varepsilon}\right)$ has negligible effect on E_{cII}.

If the fibres are to produce a material stronger than the work-hardened matrix alone, the strength of the composite must exceed the ultimate tensile strength of the free matrix, σ_{mu}, i.e.

$$\sigma_{cu} = \sigma_{fu} V_f + \sigma_m' (1-V_f) > \sigma_{mu} \qquad (6)$$

Expression (6) sets a critical V_f[1] given by:

$$V_f \text{ crit.} = \frac{\sigma_{mu} - \sigma_m'}{\sigma_{fu} - \sigma_m'} \approx \frac{\sigma_{mu}}{\sigma_{fu}}$$

for σ_{mu} and $\sigma_{fu} \gg \sigma_m'$ (7).

Only if the volume fraction of fibres exceeds V_f crit. will fibre strengthening occur.

Also, if the fibres all break in one cross-section the composite will fail unless the ductile matrix can support the load. The maximum stress that the matrix can support is σ_{mu}. The failure of all the fibres results in immediate failure of the composite only if,

$$\sigma_{cu} = \sigma_{fu}V_f + \sigma_m'(1-V_f) > \sigma_{mu}(1-V_f) \qquad (8)$$

Expression (8) defines a minimum volume fraction, $V_f$min.,[1] which must be exceeded if the strength of the composite is to be given by expression (2). Hence:

$$V_f\text{min.} = \frac{\sigma_{mu} - \sigma_m'}{\sigma_{fu} + \sigma_{mu} - \sigma_m} \qquad (9)$$

These predictions were found, by McDanels *et al.*,[9] to agree with experiments on W-Cu composites, within the limits of the scatter observed in the experimental values.

Howard[16] made investigations on steel wire-reinforced copper composites. Values of the tensile strengths predicted according to expression (2) were found to be lower than the experimental values. Hence, he proposed an expression for ultimate tensile strength by modifying expression (2). In his expression an extra term, which is a function of the fibre diameter and hardness of the fibre, was added.

Discrepancies between the experimental tensile strength and the predicted values according to expression (2) have been found by many other

investigators[10,6,8,31] working with different composite systems.

Cooper[32] obtained values of ultimate tensile strengths for different orientations of the longitudinal direction of the tungsten fibres with the specimen axis of the W–Cu composites. The ultimate tensile strengths were found to decrease with increasing angle of orientation of the fibres.

Jackson *et al.*[13] working with 50 volume per cent stainless steel–Al composites found that the ultimate tensile strengths increased up to 20° misorientation of the fibre axis with the composite axis and then decreased as the misorientation further increased.

Kelly *et al.*[11] investigated the deformation characteristics of W–Cu composites. In their work the copper matrix was incidentally a single crystal. The ultimate tensile strengths and the Young's moduli in Stage I were found to agree with the predicted values according to the rule of mixtures within the limits of scatter in the experimental values.

The predicted Young's modulus in Stage II and the stress values were found to be lower than the experimental values. Kelly *et al.*[11] using expression (3) and the experimental stress–strain curves of tungsten wire and W–Cu composite derived the matrix stress–strain curve. The derived matrix stress–strain curve did not coincide with the stress–strain curves obtained for a free copper single crystal. Kelly *et al.*,[11] Tanaka *et al.*,[33] and Neumann *et al.*[34] gave explanations for this discrepancy and predicted the slope of the Stage II of the derived matrix stress–strain curve.

C. Scope:

Kelly *et al.*[11] investigated the deformation characteristics of W–Cu composites. Their liquid–infiltration method of fabricating the W–Cu

composites incidentally also gave essentially a single crystal matrix.

For the purpose of the present investigation it was felt that deformation studies on a different composite system with a single crystal matrix of specific orientation might yield useful information regarding the work hardening behaviour of composites.

Finding a suitable system, and fabricating composites with various volume percents of fibre reinforcement, were of specific interest.

II. EXPERIMENTAL PROCEDURE

A. Selection of the Composite System:

Tungsten and stainless steel wires were chosen as reinforcing materials. Aluminum, magnesium and zinc were the possible matrix materials. It was desired that the reinforcing material and the matrix material should not have any mutual solubility. Also, the matrix should be easily grown into a single crystal in the presence of reinforcing material.

Preliminary experiments were done by melting the matrix material in a graphite crucible. The reinforcing material, in the form of wires, was kept vertically inside the molten matrix material. The matrix material was cooled in a controlled way to prevent pipe formation. This was done by lowering the crucible on to a metal block kept below the vertical tube furnace. When the crucible was lowered on to the metal block, the upper half was kept inside the furnace. The cooling furnace acted as a "hot top." When the composite casting was cold it was removed from the graphite crucible.

Using this method, W-Al, stainless steel-Al, W-Mg, stainless steel-Mg, W-Zn and stainless steel-Zn composites, with polycrystalline matrices, were obtained. A modified Bridgman technique was used to attempt to grow single crystal matrices in these composites.

Growing a single crystal matrix of magnesium was not possible. The aluminum matrix grew into a single crystal in W-Al system but not in the stainless steel-Al system. In both cases alloy formation between aluminum

and the fibres occurred; Figures 2a and 2b.

Zinc gave single crystal matrices in both systems W-Zn and stainless steel-Zn. Alloy formation between zinc and stainless steel was observed. However, alloy regions around the fibres, as seen in the stainless steel-Zn composites, were never seen in the W-Zn composites. Figures 3a and 3b show cross-sections of W-Zn and stainless steel-Zn composites.

From the preliminary experiments it was thus found that the W-Zn system was the most suitable system for experimentation.

B. Bonding Characteristics Between Tungsten and Zinc:

Bonding between the reinforcing material and the matrix material is an important aspect of composite properties and hence an effort was made to determine the wetting characteristics between tungsten and zinc using a sessile drop experiment. The experiment was unsuccessful. Evaporation of zinc at or near the melting point due to its high vapour pressure was the principal problem. Hence, an attempt was made to determine directly the bond shear strength between tungsten and zinc, using the fibre "pull out" experiment.

In the "pull out" experiment, a single tungsten wire was pulled out of the zinc matrix using an Instron machine. The "pull out" experiment was also unsuccessful in that reproducible results could not be obtained, and the scatter in results was extremely large.
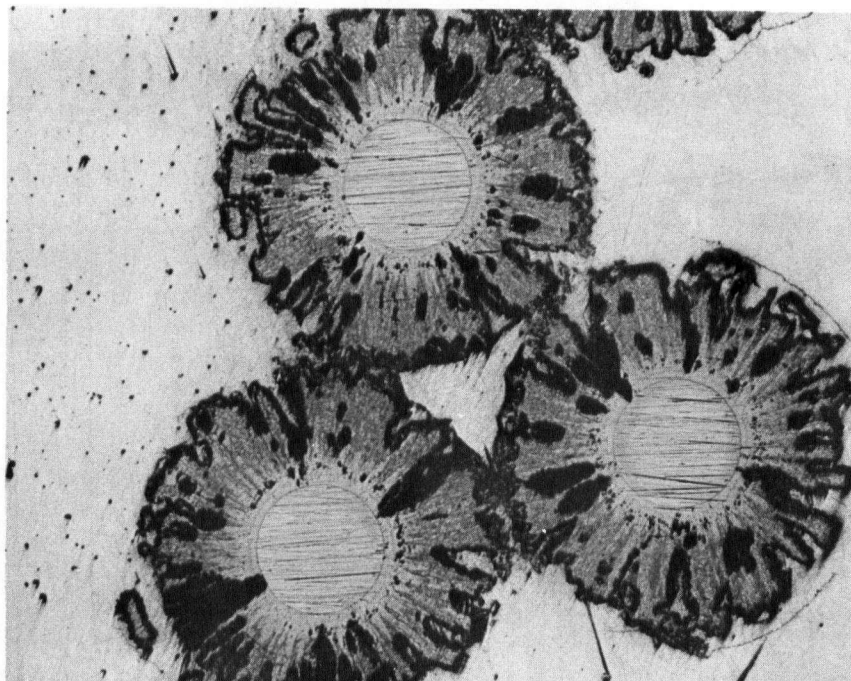
Fig. 2a.   Cross-section of a W-Al Composite, 10% Sodium Hydroxide Etch, X23
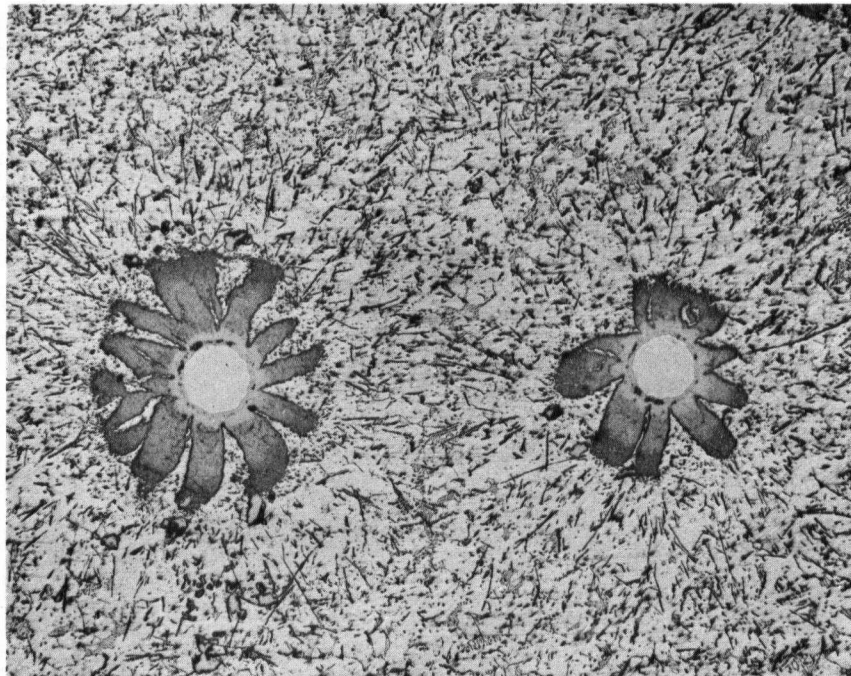
Fig. 2b.   Cross-section of a Stainless Steel-Al Composite, 10%
Sodium Hydroxide Etch, X23.
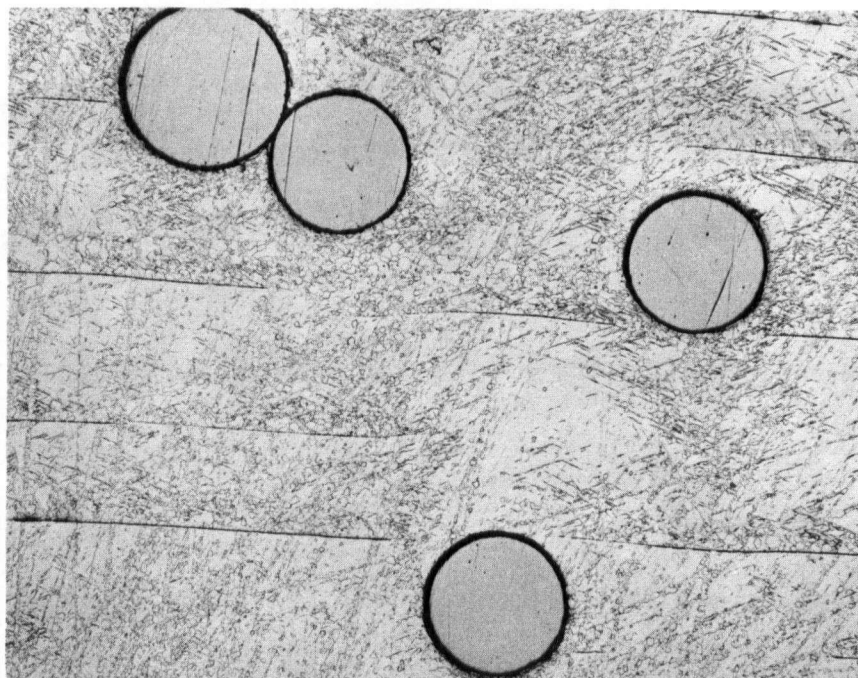
Fig. 3a. Cross-section of a W–Zn Composite, Zinc Etch, X23.
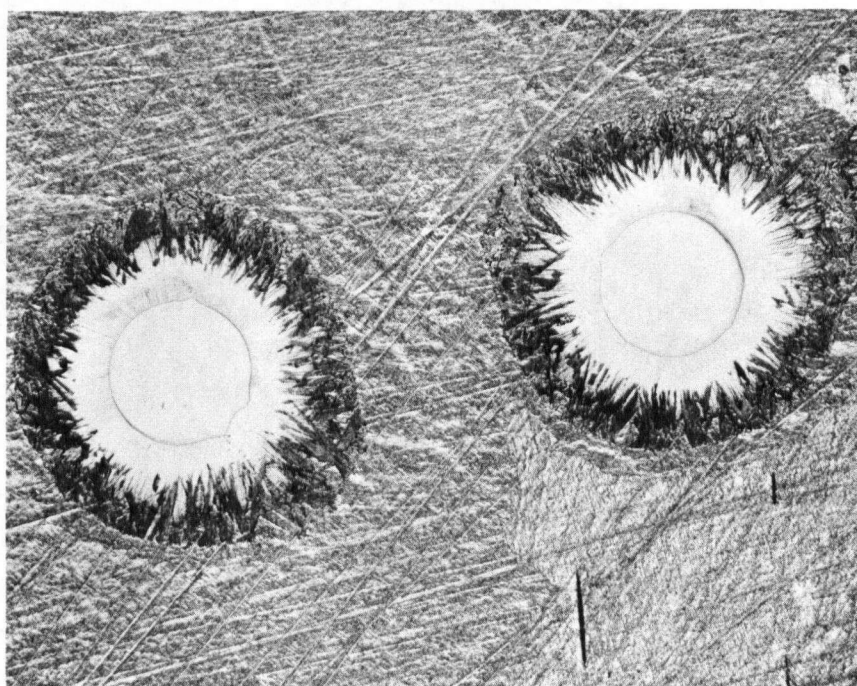
Fig. 3b. Cross-section of a Stainless Steel–Zn Composite, Zinc Etch, X23.

C. Fabrication of W-Zn Composites:

Initially, liquid metal infiltration of bare W-wires was used to obtain W-Zn composites. On sectioning the composites thus obtained, it was found that all the tungsten wires were together and there was no trace of zinc between the wires. Hence this method of fabrication was considered unsuitable.

Liquid metal infiltration of tungsten wires with electrodeposited zinc coatings was found to be the most successful method of fabrication of W-Zn composites. For electrodeposition of zinc on W-wires the acid electrolyte used was:[35]

$ZnSO_4 \cdot H_2O$	240 gms/litre
Na_2SO_4	40 gms/litre
$ZnCl_2$	10 gms/litre
H_3BO_3	5 gms/litre
Distilled water	1 litre
pH	3-4
Temp.	30°C.

Anodes were obtained by hot rolling 99.99% pure zinc blocks, at 150°C.[36] into 10 cm x 27 cm x 0.25 cm plates.

Tungsten wire, 0.01 inch in diameter, was wound on 27 cm x 13 cm plastic frames. The W-wire was cleaned using an HF + HNO_3 acid solution. Tungsten wire wound on the frame acted as the cathode. An average wire diameter was determined, using a travelling microscope, prior to the deposition. Zinc was deposited onto the wires at a cathode current density of 75 amps/ft^2. The thickness of the deposit was adjusted as needed. The deposited

wire was then immersed in a solution of 50% HNO_3 acid to get a shiny surface, rinsed in distilled water and dried by natural evaporation overnight.

Zinc-coated tungsten wires were cut into 25-cm long pieces which were bundled together. A bundle was put inside an aquadag (colloidal suspension of graphite in water) coated pyrex tube of 6 mm inner diameter. The number of coated wires bundled depended on the volume fraction of fibres desired in the composite. The bundle was kept in the middle of the pyrex tube. The tube was constricted near both ends of the fibre bundle.

One end of the tube was immersed in molten zinc (99.999% pure) and the other end was connected to suction. The bundle was kept hot at 250 - 300°C. by means of an induction heating coil. When the bundle was hot the molten metal was infiltrated into the bundle. Induction heating was switched off as the molten metal completely covered the bundle. The induction coil then acted as a cooling coil. Figure 4 shows a schematic diagram of the liquid metal infiltration set-up. W-Zn composites thus obtained had a polycrystalline zinc matrix.

D. Method of Growing Oriented Single Crystals of Zinc and Zinc Matrix:

Randomly oriented zinc crystals were grown using 99.999% pure zinc supplied by COMINCO (B.C. Trail, Canada). The modified Bridgman method was used to grow 6 inch long x 1 1/8 inch diameter zinc crystals. The maximum temperature in the furnace was about 450°C. The growth rate was 3 cms/hour.
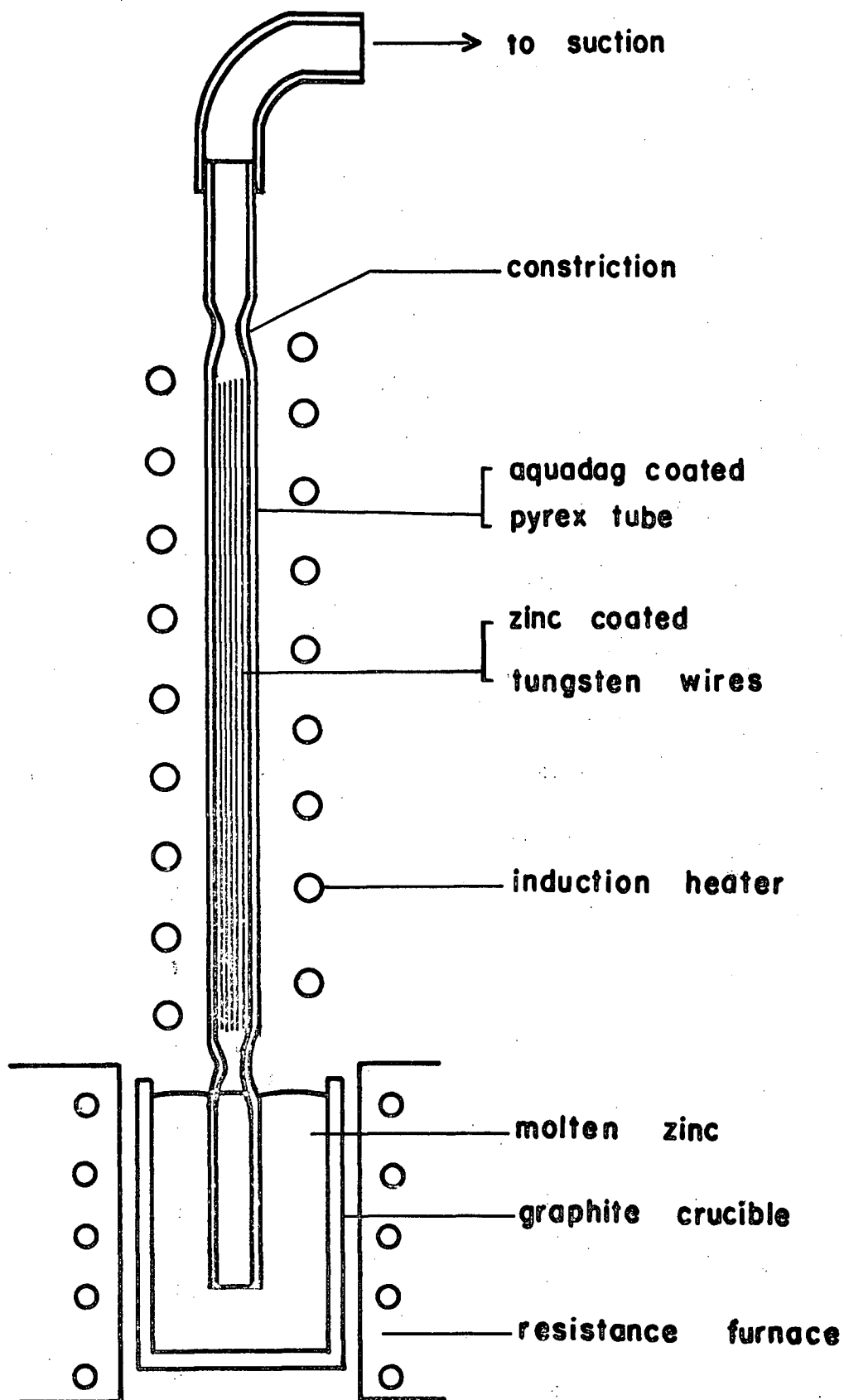
Fig. 4. Schematic Diagram of the Liquid Metal Infiltration
Set Up.

Seed crystals of circular cross-sections with basal plane orientation of 45° to the long axis were cut from the bulk crystals using the spark erosion method. Basal plane cleavage to a depth of 1-2 mms, due to spark damage, was seen in the seed crystals.

Polycrystalline zinc rods of 3/8 inch diameter x 12 inches long were obtained by swaging 5/8 inch diameter pure zinc castings at 200°C. The seed crystal and the cleaned polycrystalline zinc rod were put inside an aquadag coated pyrex tube and vacuum sealed. The polycrystalline rod was then grown into an oriented single crystal using the modified Bridgman technique. The maximum temperature in the vertical crystal growing furnace was 450 $\pm$ 10°C. The growth rate of the crystal was 2 cms/hr. The crystal was recovered from the pyrex tube by dissolving away the tube in 52% HF acid.

The same procedure was followed to grow oriented single crystal matrices of zinc in W-Zn composites. In this case, pyrex tubes with 6 mm inner diameter were used. Also, polycrystalline zinc rod was replaced by the W-Zn composite.

Oriented free crystals and composite crystals were cleaned using 50% HNO_3 acid. The orientations of the crystals were checked by the back-reflection Laue X-ray method.

E. Preparation of W-Zn Composites With 0.0015 Inch Diameter Tungsten Wires:

Tensile tests carried out on W-Zn composites containing 0.01 inch diameter W-wires showed a 3-6 mm length "pull out" of the tungsten wires on the fractured surface. This is because the load bearing capacity of the fibre is greater than the load bearing capacity of the fibre-metal

interface. The smaller the diameter of the fibre, the smaller is the load bearing capacity of the fibre. The use of fibres with smaller diameter minimizes fibre pull out. Hence 0.0015 inch diameter tungsten wires supplied by SYLVANIA (Chem. and Met. Div., Towanda, Pa.) were subsequently used for reinforcing.

The procedure adopted to prepare W-Zn composites of single crystal matrix with 0.0015 inch diameter tungsten wires was the same as that with 0.01 inch tungsten wires.

For the fabrication of composites containing 6, 12, 25, 100 and 186 wires, the electrodeposited wires were bundled together with thin strips of pure zinc prior to liquid metal infiltration.

The composites prepared contained 6, 12, 25, 100, 186, 372, 743 and 1486 tungsten wires, of average diameter 0.0329 mm, in a cross-section of 26-28 mm^2. The orientations of the zinc matrices involved were χ_o = 35-45° and λ_o = 35-49°. χ_o is the angle between the slip plane (0001) and the tensile axis of the specimen. λ_o is the angle between the most favourable slip direction [11$\bar{2}$0] and the tensile axis of the specimen.

Back reflection Laue X-ray pictures showed the absence of low angle boundaries in the matrix of the W-Zn composites.

F. Tensile Tests:

Pure zinc crystal and W-Zn composite test specimens, 3 inches long, were annealed at 400°C. for one hour. Test specimens of 0.0015 inch diameter tungsten wire were annealed at 450°C. for one day. The test specimens were then tested in an Instron tensile testing machine at a cross-

head speed of 0.02 inch per minute on a 2 inch gauge length. Load-elongation curves were recorded on an x-y recorder at suitable chart speeds.

The wire and the composite specimens were mounted on the machine using split grips. The pure zinc crystal specimens were mounted on the machine using brass holders soldered to the specimens.

For wire specimens, elongation was recorded according to the cross-head movement. An extensometer was not used because the W-wire was not strong enough to support it.

In the case of pure zinc crystals, elongation was measured according to the movement of cross-head.

In the earlier tests, the elongation of the composites was recorded according to the cross-head movement of the Instron machine. In later experiments elongations were recorded according to the strain gauge extensometer. Also, all the tests with composite specimens were repeated using a 1 inch gauge length extensometer to measure elongation. The use of the strain gauge clearly showed four stages of deformation in the load-elongation curves as described earlier.

G. Control Experiment to Examine the Behaviour of W-Zn Composite in Stage II:

Control experiments were conducted to check whether the composites in stage II are plastic or elastic. W-Zn composite specimens were stressed into stage II and then unloaded. The initial part of the unloading curve was parallel to the elastic-elastic line, demonstrating that the matrix in stage II behaves plastically. A curve obtained from the control experiment is shown schematically in Figure 5.
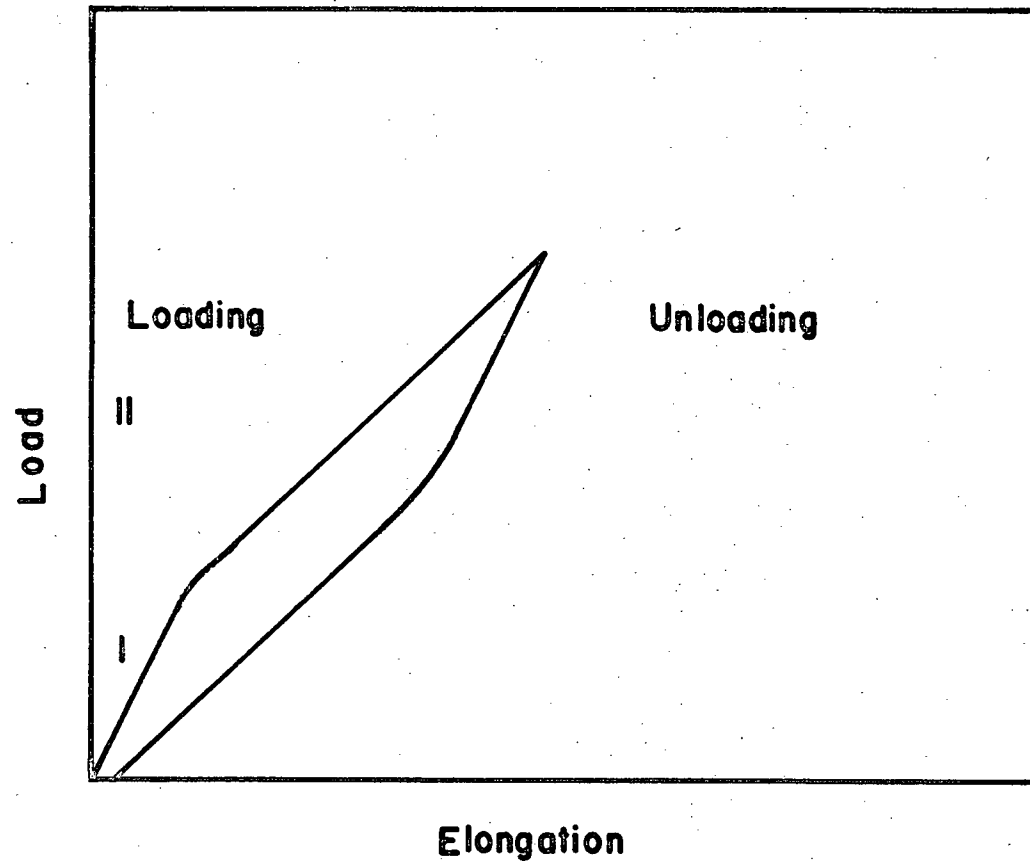
Fig. 5. Schematic Diagram of the Load-elongation Curve of a W-Zn Composite Obtained in the Control Experiment.

H. Volume Fraction of Fibres:

The volume fraction of fibres, in each composite, was calculated from the fibre diameter, the number of fibres and the diameter of the composite.

III. RESULTS

A. Metallographic Observations:

A.1. Slip Lines and Twinning in Deformed Zinc Single Crystals:

An attempt was made to observe the slip and twin markings on the surface of the fractured zinc crystal. Figure 6 shows the slip lines and twins on the surface of a crystal. No secondary slip lines are seen. Twinning might be responsible for the serrations in the later stages of the load-elongation curves. Serrations were also observed in those composites, which behaved like a single crystal, in the final stages of deformation. Since the surfaces of the composites were not good enough for optical examination, no photographs were taken.

A.2. Microscopic Observations of the as made Composite:

Composite specimens were spark-cut for metallographic examination. The cross-sections were ground and polished using the diamond polishing wheel. The polished cross-sections were viewed under the microscope to see the fibre distributions. It has been stated[1] that poor wettability between the fibers and the matrix would develop voids inside the composites. Microscopic examination did not show any voids in the composites. Typical macrographs of the cross-sections for two composites are given in Figures 7a and 7b.

In some cross-sections oxide rings were seen encircling the tungsten fibres. This can be accounted for by the inability to use any sort of protective atmosphere while heating the electrodeposited tungsten wires prior to infiltration. The continuity of the oxide rings was investigated.

23
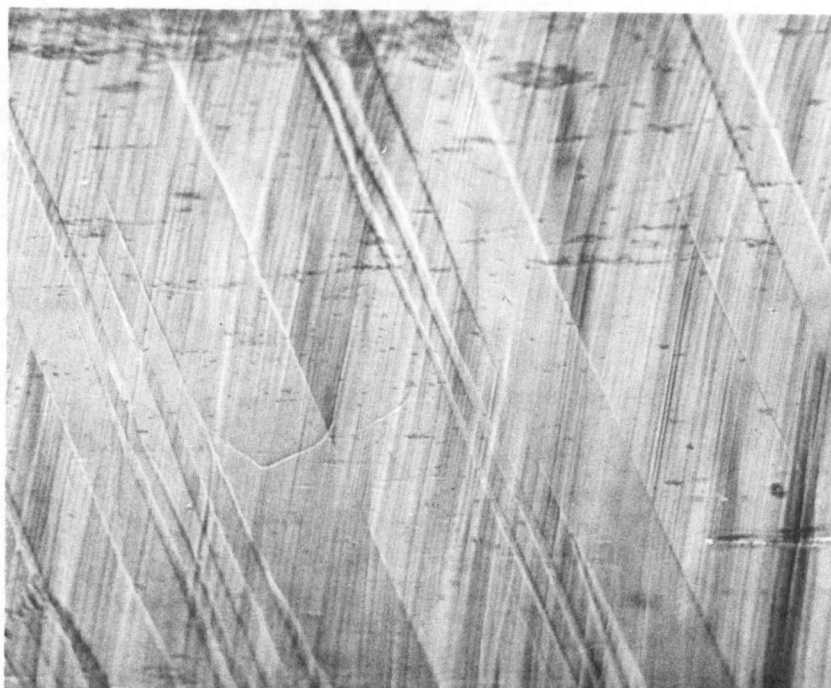
Fig. 6.   Slip Lines and Twin Markings on the Surface of a
Deformed Zinc Crystal, X130.
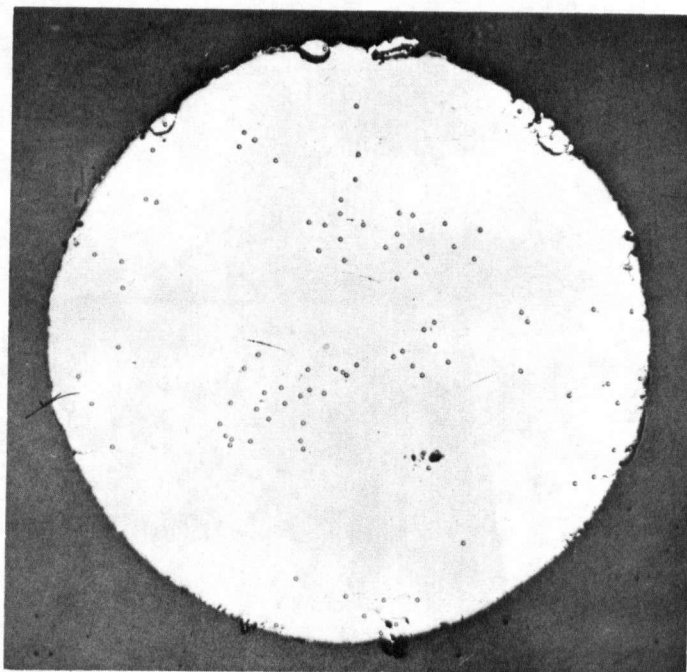
(a)
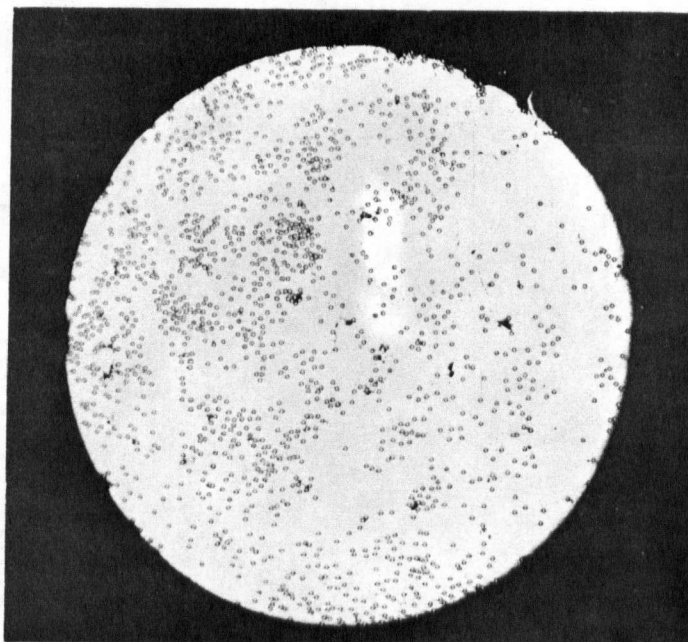
(b)

Fig. 7. Distribution of Fibres in a W-Zn Composite Containing
(a) 100 Tungsten Wires, (b) 1486 Tungsten Wires, X12.

The polished specimen surface was etched with modified Gilman's solution:[36]

$$320 \text{ gms } CrO_3$$

$$20 \text{ gms } Na_2SO_4$$

$$1000 \text{ mls } H_2O$$

Figure 8a shows discontinuities in the oxide rings. It should be noted that all the fibres did not have the oxide rings encircling them. Longitudinal sections of the composites were polished and examined. The oxide layer is discontinuous as shown in Figure 8b. Etching of the longitudinal section was avoided because the increased etching rate in the direction of the oxide layer itself tended to produce continuity.

Incidentally the twins formed during grinding and polishing operations showed the continuity of the crystal matrix, by running parallel, inside and outside the oxide rings (Figure 8a).

A.3. Fractographic Observations:

Tungsten-zinc composites containing up to 0.08 volume per cent fibres fractured essentially the same as the pure zinc single crystal. Composites containing higher than 0.08 volume per cent fibres fractured by cleaving through the basal planes. The cleaved surface due to composite fracture was observed under the microscope. Twins in large numbers are seen in the matrix in the vicinity of the fibres as shown in Figures 9a and 9b. The twin density increased with the volume fraction of the fibres in the matrix.

Also, fractographic observations were made using the scanning electron microscope. A typical scanning electron micrograph is shown in Figure 10. Steps can be seen connecting two fibres in the micrograph.
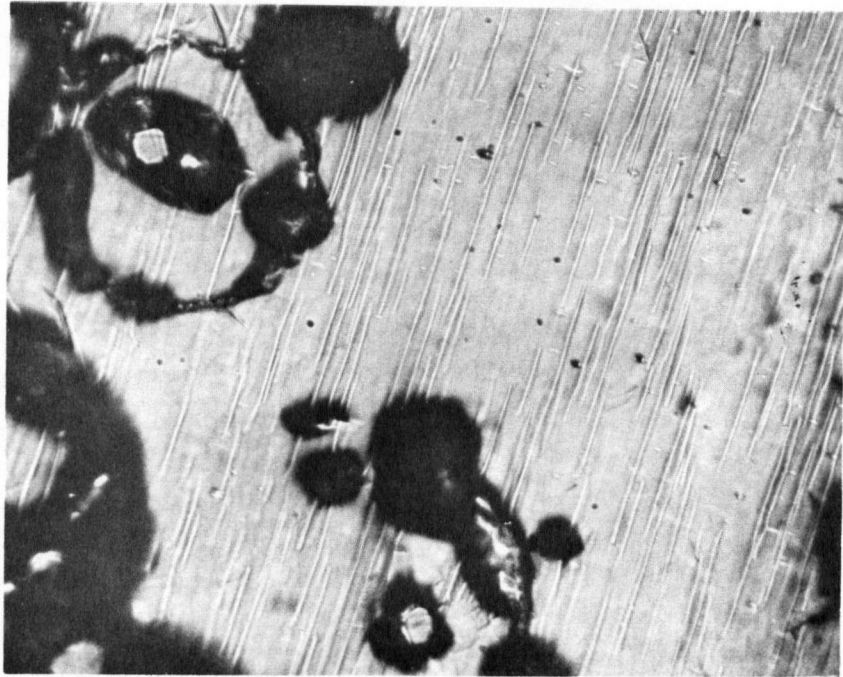
Fig. 8a. Cross-section of a W-Zn Composite Showing Oxide-rings and Twins, X125.
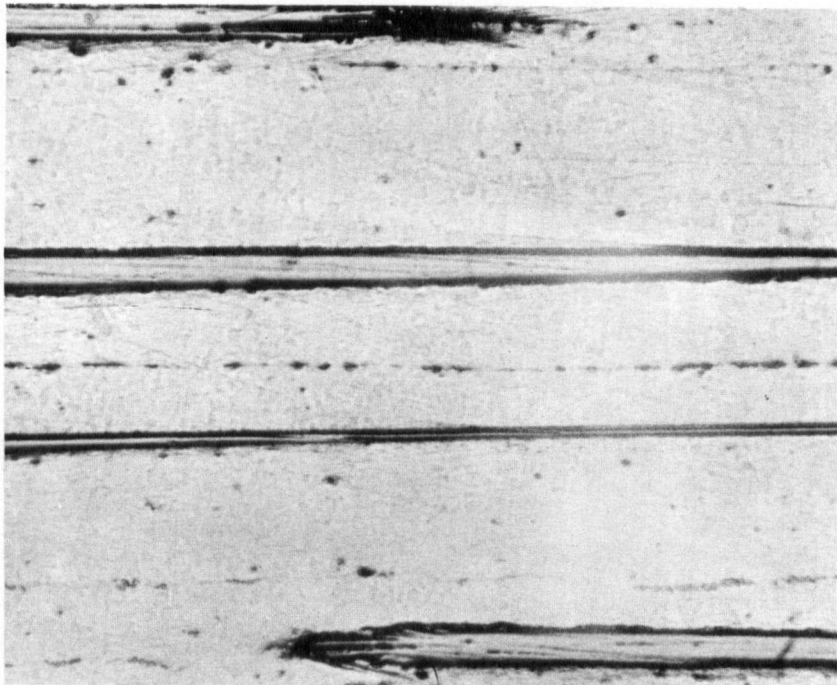
Fig. 8b. Longitudinal-Section of a W-Zn Composite Showing Discontinuity in the Oxide-layers, X110.
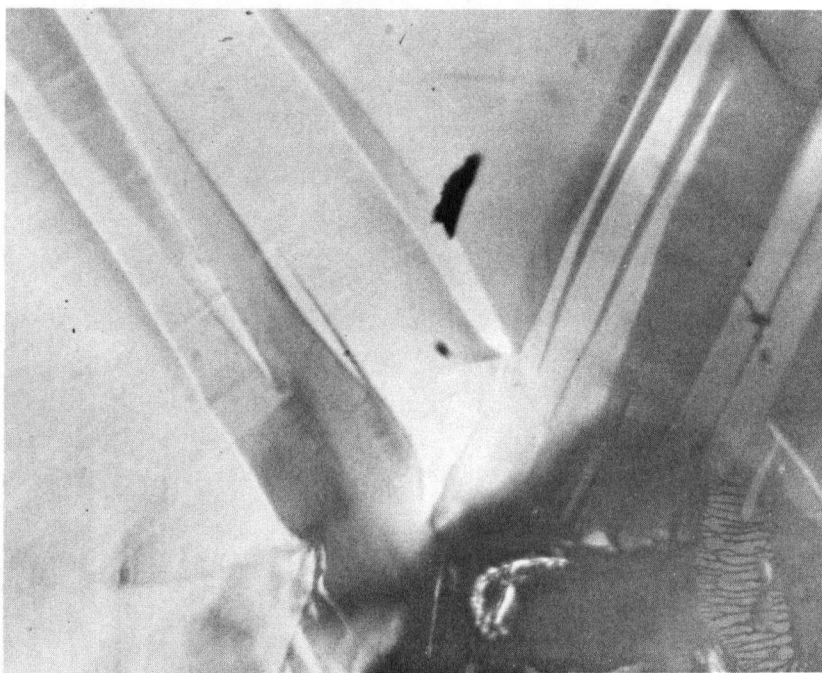
(a)
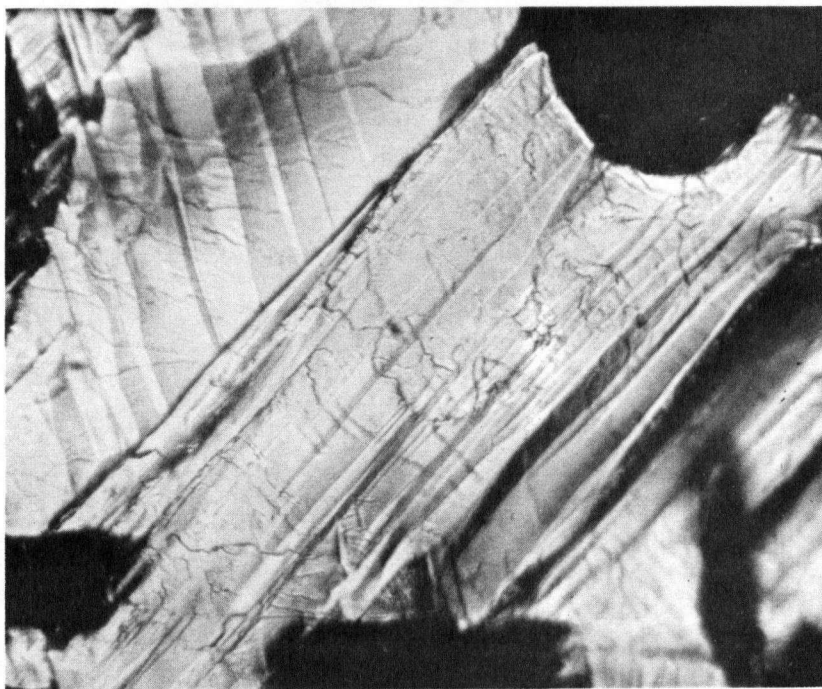
(b)

Fig. 9. Twin Markings on the Fractured Surface of W–Zn Composite
Containing (a) 100 Tungsten Wires, (b) 1486 Tungsten Wires,
X275.
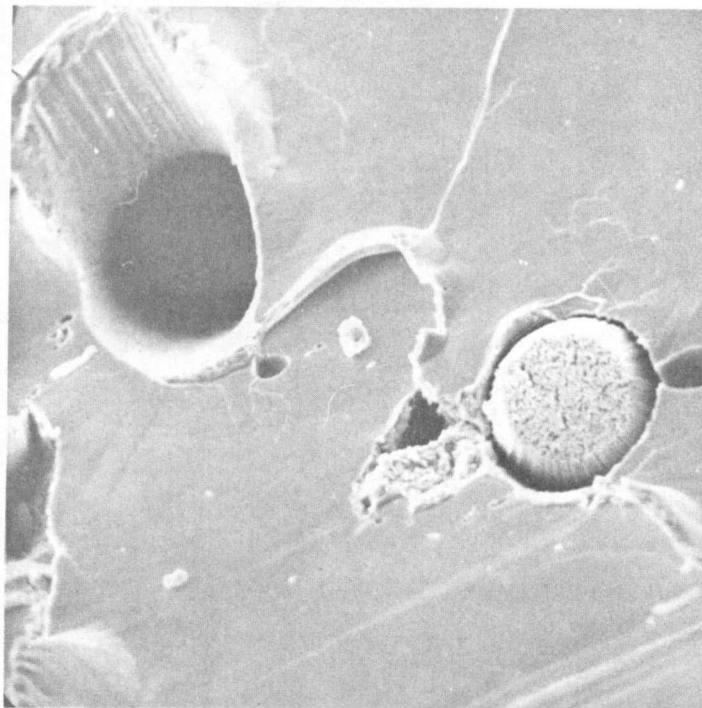
Fig. 10. Scanning Electron Micrograph of the Fractured Surface of a W–Zn Composite Containing 743 Tungsten Wires, X715.

A.4. Observations on Fibres Deformed to Fracture:

Free tungsten fibres deformed to fracture showed a single necking at the fracture end. To investigate deformation behaviour of the fibres inside the matrix, some of the composite specimens deformed to fracture were etched to extract the fibres from the matrix using 50% nitric acid.

One of the specimens which deformed essentially as a pure zinc crystal, was treated as described above. Small lengths of fractured fibres were recovered. The length of the bits varied from 1 to 5 mms. When these bits were viewed using transmitted light under the optical microscope they exhibited multiple necking profiles on the surface. The multiple neckings were present near both fractured ends of the fibres. Figures 11a and 11b show the length of the bits and the multiple necking.

The other specimens, which fractured by cleaving through the basal plane, left behind continuous fibres on etching off the matrix. This shows that the fibres did not fracture inside the matrix prior to the specimen fracture. Also multiple necking was seen in the fibres near the fractured ends. The multiple necking was seen only in those composites which deformed greater than the free tungsten fibre tested.

A.5. Electron-Probe Analysis of the Fibre-Matrix Interface in a W-Zn Composite:

It has been stated[37] that alloy formation between fibres and the matrix at the interface deteriorates the properties of the fibre and hence of the composite. In the present W-Zn system, it is stated that the mutual solubilities between the components of the system is essentially nil[37] below 1350°C.[38] To confirm this, electron-probe analysis of a W-Zn composite was carried out.
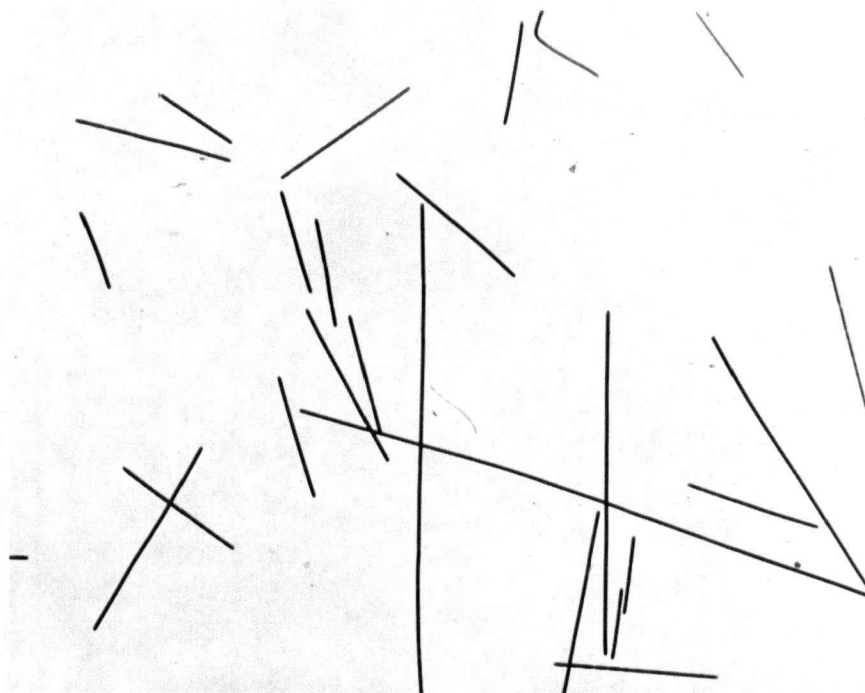
Fig. 11a.   A Portion of the Extracted Tungsten Wire Fragments Obtained
by Dissolving the Matrix of a Fractured W-Zn Composite Con-
taining 6 Tungsten Wires, x 12.
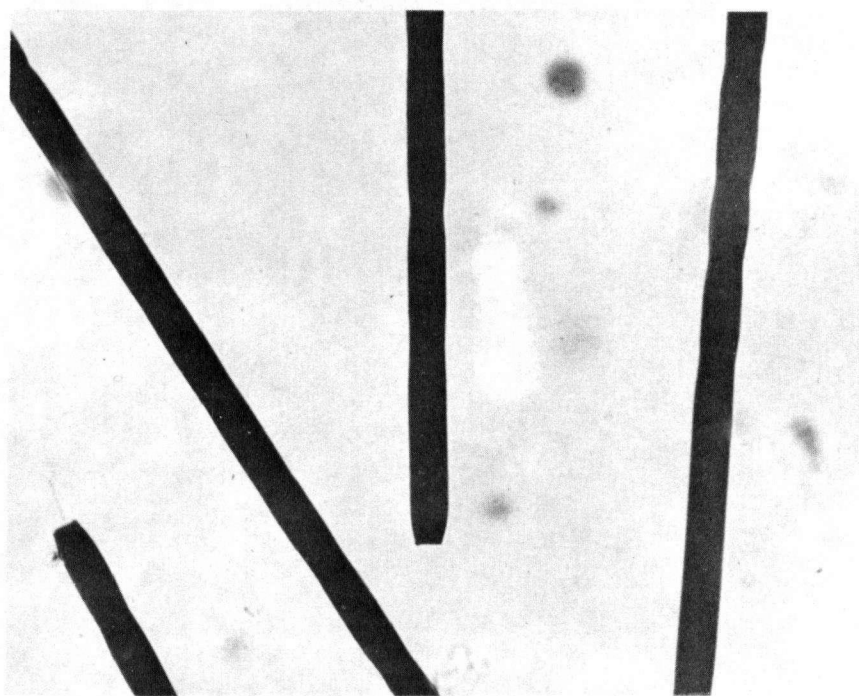
Fig. 11b.   Multiple Necking in the Fragments, X 130.

A polished cross-section of the W-Zn composite was continuously scanned, in and out of a single fibre, along the diametric axis of the fibre. The scanned path-composition curve was recorded on an x-y recorder. The scanned path-composition curve obtained showed, with a resolving capacity of the electron-probe equal to one micron, no mutual solubility between tungsten and zinc. The scanned path-composition curve obtained for the W-Zn system is given in Figure 12.

B. Tensile Properties:

B.1. True Stress-True Strain Curve for Tungsten Wires (Polycrystalline):

Tensile properties like stress, strain and elastic constants are of great importance in theoretical predictions. Also, the tensile properties of the materials vary with the fabrication methods by which they are obtained. Hence, an average true stress-true strain curve was plotted for 0.033 mm diameter tungsten wire. This curve is obtained from the load-elongation curves of the tungsten wires using the relations:

$$\sigma_f = \frac{P}{A_o} (1 + \frac{\Delta l}{l_o})$$ (10)

and

$$\varepsilon_f = \ln (1 + \frac{\Delta l}{l_o})$$ (11)

where

σ_f = the true stress;

ε_f = the true strain;

l_o = the original gauge length;

P = the tensile load

Composition

Zn   W   Zn

←

10 μ

Scanned-path (Distance)
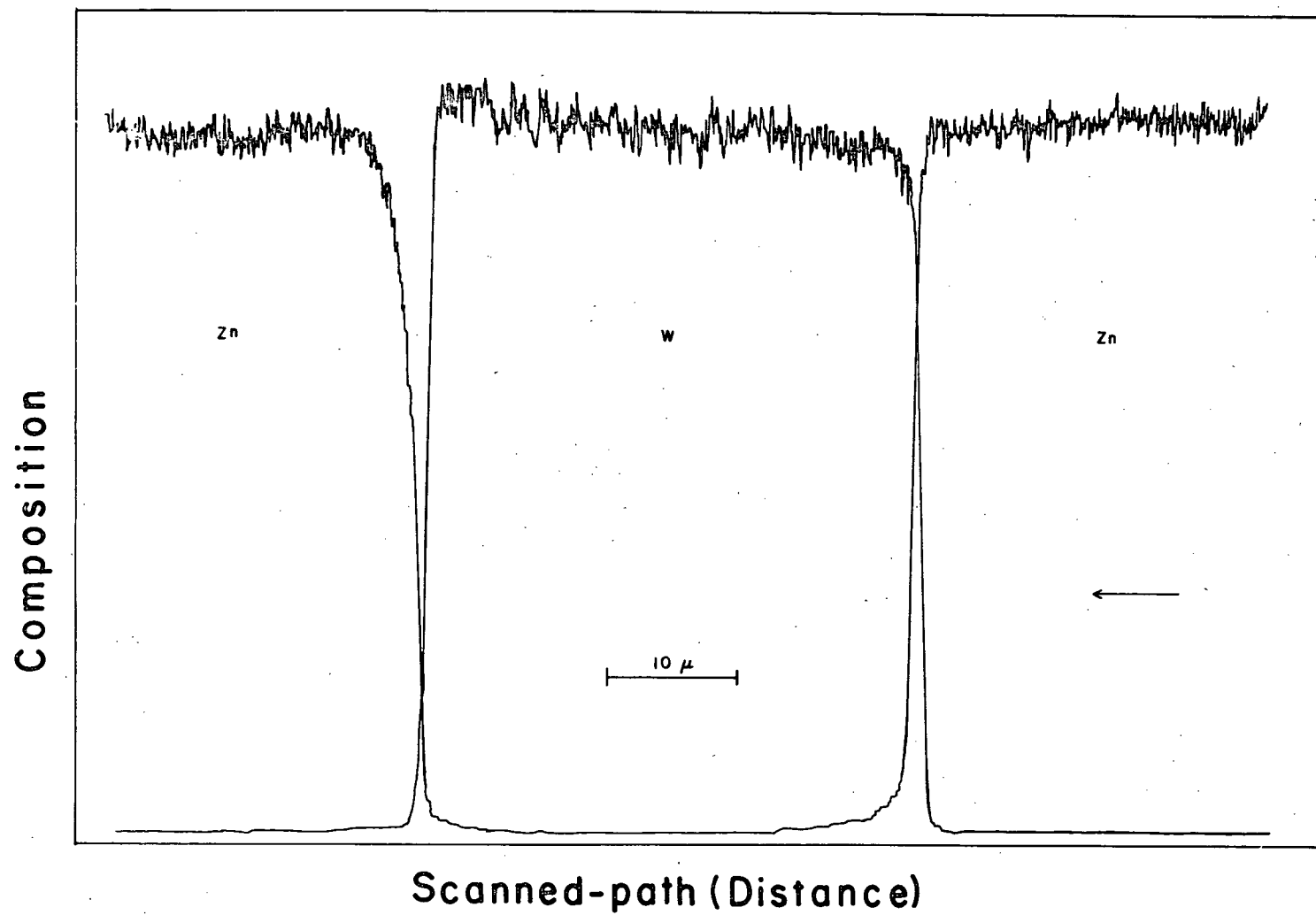
Fig. 12. Composition-distance Curve Obtained from Electron-probe Analysis.

and   Δl =   the total elongation at P according to the cross-head
               movement of the Instron tensile testing machine.

Figure 13 gives the average true stress-true strain curve for polycrystalline tungsten wire. This curve is an average of the load-elongation curves obtained for three wire specimens. All the specimens fractured at a strain of 2% and the results were reproducible.

From the stress-strain curve of tungsten wire the yield stress σ_{fy}, the Young's modulus E_f, and the ultimate tensile strength σ_{fu} are obtained. These values are given in Table 5a, and 3.

Yield stress is defined to be the stress at which the stress-strain curve first deviates from linearity. Young's modulus is the slope of the linear portion of the stress-strain curve. The ultimate tensile strength is defined to be the maximum stress in the stress-strain curve.

The reason for obtaining elongation according to the cross-head movement is that the wire was too thin to support an extensometer. The value of E_f obtained from the stress-strain curve is comparable to the value obtained by Kelly et al.[11] Since mechanical properties vary according to the manufacturing method the available data are not used except for the Poisson's ratio ν_f.

The E_f value obtained experimentally and ν_f value taken from Lowrie and Gonas[39] were used to obtain the shear modulus G_f, the bulk modulus K_f and the plane strain bulk modulus k_{fp} of the tungsten wires. The relations used are:

$$G_f = \frac{E_f}{2(1 + \nu_f)} \qquad (12)$$

$$K_f = \frac{E_f}{3(1 - 2\nu_f)} \qquad (13)$$

and
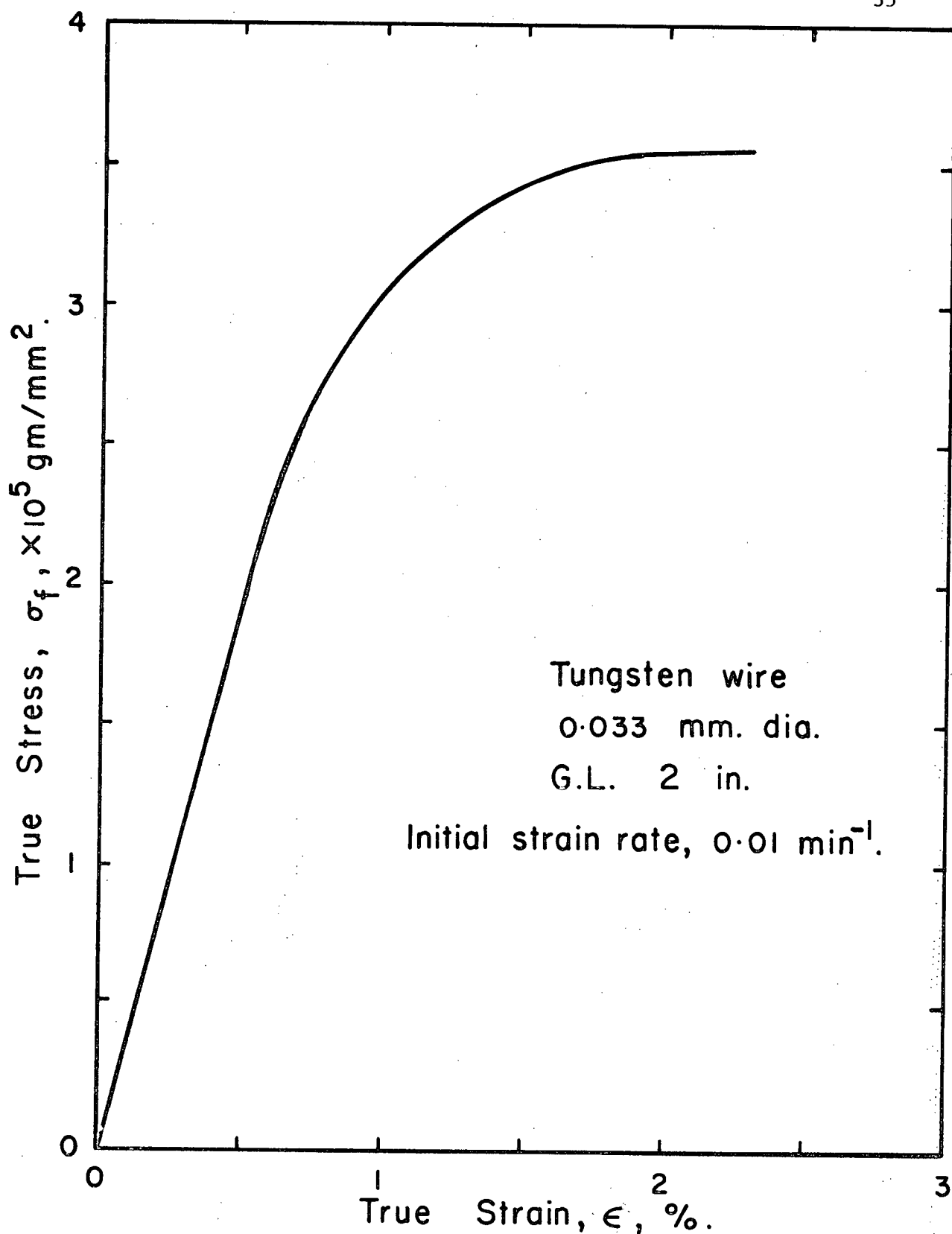
Fig. 13. True Stress-Strain Curve of a Tungsten Wire.

$$k_{fp} = \frac{3K_f}{2(1 + \nu_f)} \tag{14}$$

assuming a homogeneous isotropic solid.

The experimental and calculated values of elastic constants for tungsten wires are tabulated along with the published values of Lowrie et al.[39] and Kelly et al.[11], in Table 3.

TABLE 3

ELASTIC CONSTANTS FOR TUNGSTEN WIRE

	PRESENT CALCULATIONS	LOWRIE et al.[39]	KELLY et al.[11]
E_f	3.6×10^7 gms/mm^2	4.1×10^7 gms/mm^2	10 μ-w: $(36.4 \pm 5)10^6$ gms/mm^2 20 μ-w: $(38.1 \pm 2)10^6$ gms/mm^2
G_f	1.4×10^7 gms/mm^2	1.6×10^7 gms/mm^2	------
K_f	2.7×10^7 gms/mm^2	3.1×10^7 gms/mm^2	------
ν_f	-----	0.28	------
k_{fp}	3.2×10^7 gms/mm^2	-----	------

The values of the elastic constants given in Table 3 were used in the theoretical calculations.

B.2. True Stress-True Strain Curve for Pure Zinc Crystal and Tungsten-Zinc Composites:

With a view to examining the deformation characteristics, and hence correlating the experimental results with the theoretically predicted results, true stress-true strain curves were drawn for pure zinc crystals and tungsten-zinc composites. True stress-true strain curves are more appropriate than engineering stress-strain curves even though at low strains the difference between the two is negligibly small.

In the beginning, tensile tests were performed without using the extensometer strain gauge. The elongation was recorded according to the cross-head movement. Later, experiments were conducted using an extensometer for elongation measurement. The load-elongation curves obtained from these two methods for similar materials show that the elastic elongation recorded according to the cross-head movement is much larger than the one recorded by using the extensometer. Also, the elastic elongation recorded using an extensometer is too small on the chart to make any precise calculation of the strain or the elastic modulus of the material. Hence the Young's moduli of the pure zinc crystal and of W-Zn composites were made use of in calculating the appropriate elastic elongations.

The Young's modulus of zinc crystals was obtained using the elastic compliances. The Young's modulus of zinc varies according to the orientation of the crystallographic axis-c with the tensile axis. In particular, the Young's modulus E_m of a zinc crystal rod, the length of which makes an angle Θ with the c-axis of the h.c.p. lattice is given by:[40]

$$\frac{1}{E_m} = (S_{11}+S_{33}-2S_{13}-S_{44})\cos^4\Theta + (2S_{13}+S_{44}-2S_{11})\cos^2\Theta + S_{11} \quad (15)$$

where

S_{11}, S_{13}, S_{33} and S_{44} are the elastic compliances.

The values of the five elastic compliances for zinc taken from Wert et al.[41] for calculation purposes are:

$$S_{11} = 8.38 \times 10^{-13} \text{ cm}^2/\text{dyne}$$

$$S_{12} = 0.5 \times 10^{-13} \text{ cm}^2/\text{dyne}$$

$$S_{13} = -7.31 \times 10^{-13} \text{ cm}^2/\text{dyne}$$

$$S_{33} = 28.3 \times 10^{-13} \text{ cm}^2/\text{dyne}$$

and

$$S_{44} = 26.1 \times 10^{-13} \text{ cm}^2/\text{dyne}.$$

All the specimens, either zinc single crystals or composites with a zinc single crystal matrix, had their orientation of the basal plane with the tensile axis, χ_o, lying between 37° and 44°. An average value of $\chi_o = 40°$ and hence $\Theta = 50°$ was used in the calculation of E_m.

Also the rigidity modulus G_m, the bulk modulus K_m and the Poisson's ratio ν_m, for zinc crystals with $\chi_o = 40°$, were calculated using the relations:[40]

$$\frac{1}{G_m} = S_{44} +[(S_{11}-S_{12})-1/2S_{44}](1-\cos^2\Theta) + 2(S_{11}+S_{33}-2S_{13}-S_{44})\cos^2\Theta(1-\cos^2\Theta)$$

$$(16)$$

$$\frac{1}{K_m} = S_{33} + 2(S_{11} + S_{12}) + 4S_{13} \quad (17)$$

and

$$\nu_m = -\frac{S_{13}}{S_{33}} \text{ (approximately)} \quad (18)$$

The values of the elastic constants obtained for the zinc crystal ($\chi_o = 40°$) are given in Table 4.

TABLE 4

ELASTIC CONSTANTS FOR ZINC CRYSTAL

E_m	9.5×10^6 gms/mm^2
G_m	2.8×10^6 gms/mm^2
K_m	6.0×10^6 gms/mm^2
ν_m	0.26

These values of the elastic constants of a zinc crystal are useful in the theoretical predictions involved.

The Young's modulus of a composite, which is defined to be the Young's modulus in stage I, is obtained using expression (4).

True stress-true strain curves were obtained from load-elongation curves of pure zinc crystals using the relations:

$$\sigma_m = \frac{P}{A_o}(1 + e_T) \qquad (19)$$

$$\varepsilon_m = \ln (1 + e_T) \qquad (20)$$

and

$$e_T = \frac{\Delta l_T}{l_o} = \frac{\Delta l_e + \Delta l_p}{l_o} = \frac{P}{A_o E_m} + \frac{\Delta l_p}{l_o} \qquad (21)$$

where

σ_m = the true stress

ε_m = the true strain

e_T = the total engineering strain

A_o = the original area of cross-section

l_o = the original gauge length

P = the tensile load

Δl_T = total elongation at P

Δl_e = elastic elongation at P

Δl_p = plastic elongation at P.

The elastic strain at P was obtained using the relation

$$\frac{\Delta l_e}{l_o} = \frac{P}{A_o E_m}$$ (22)

Similarly, true stress-true strain curves were obtained from the load-elongation curves of composites using the relations given for pure zinc crystals and replacing σ_m, ε_m and E_m by σ_c, ε_c and E_{cI} respectively. For composites Δl_e corresponds to the elastic-elastic elongation and $\Delta l_p = \Delta l_T - \Delta l_e$.

Figures 14a and 14b show true stress-true strain curves for specimens X-7, C-16, C-14, C-25, C-20, C-27, C-40, C-9 and C-55. X and C represent crystal and composite specimens respectively. Similar curves were also obtained for other specimens. The curves obtained for W-Zn composites show four stages of deformation as observed by McDanels et al.[9] in W-Cu composites.
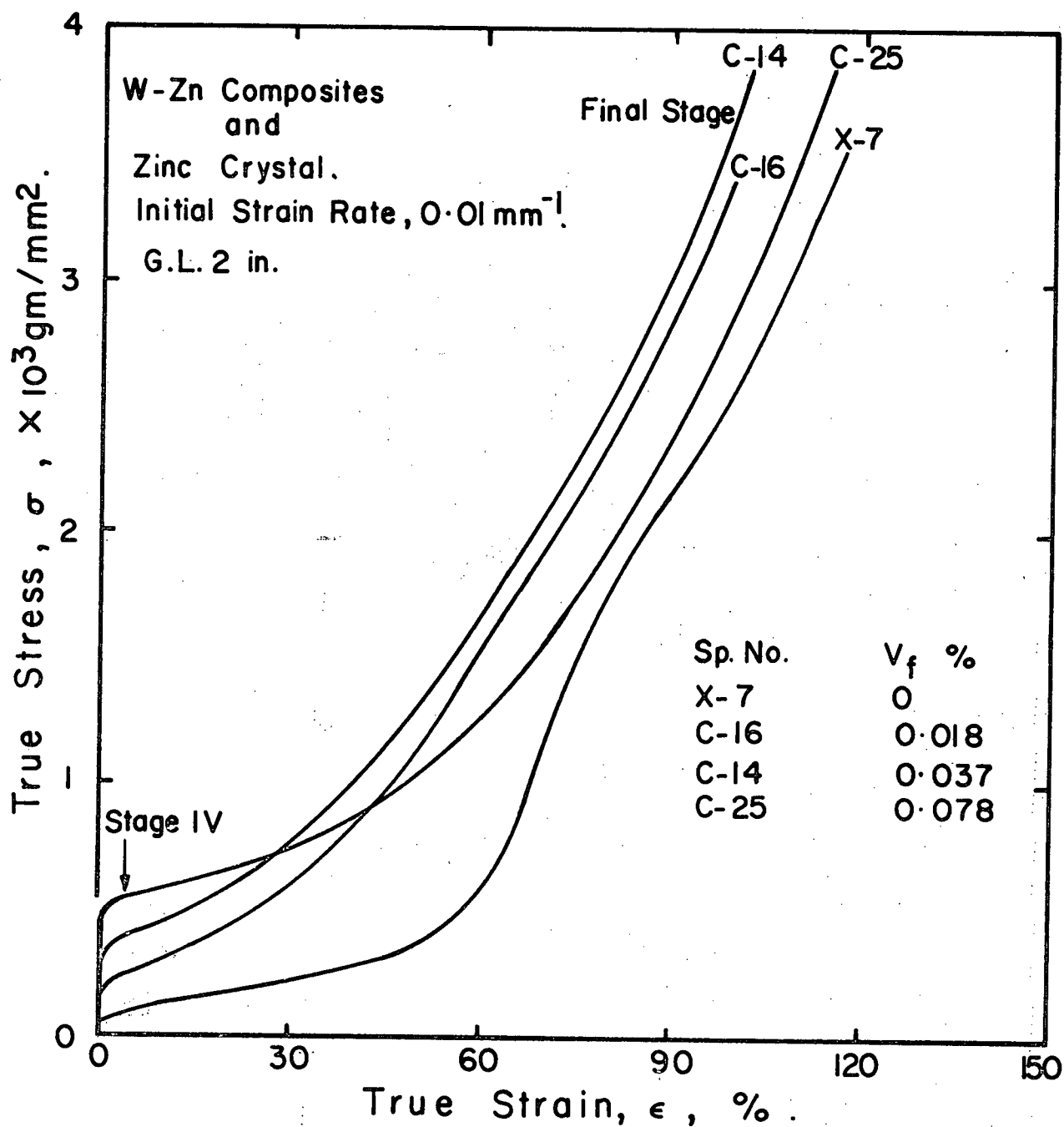
Fig. 14a. True Stress-strain Curves of Zinc Crystal and W-Zn
Composites.
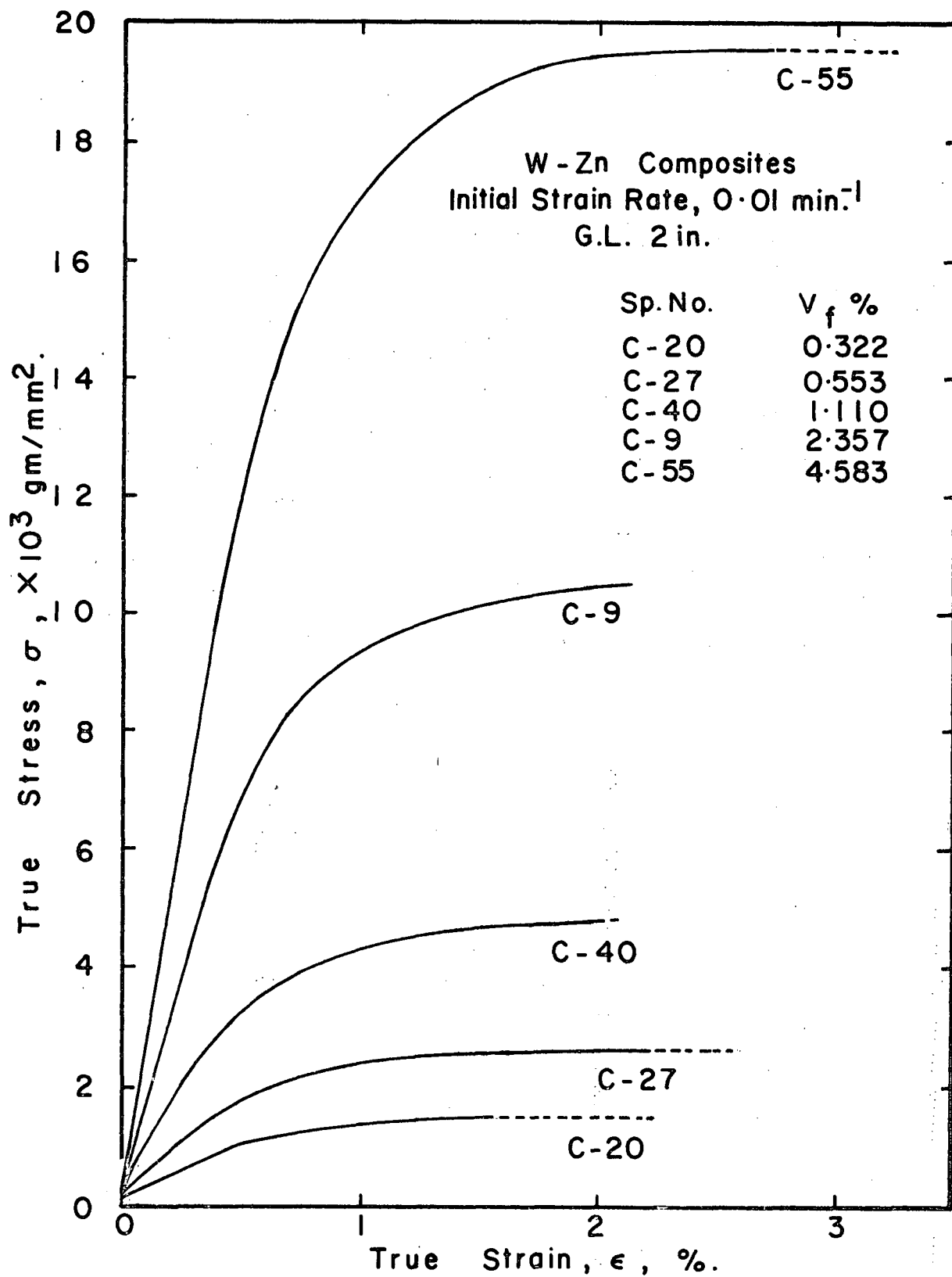
Fig. 14b. True Stress-strain Curves of W-Zn Composites.

Curves obtained for the composites containing up to 0.08 volume

per cent tungsten fibres were similar to those of pure zinc crystals. Ser-

rations were found in the final stages of the load-elongation curves of

pure zinc crystals and W-Zn composites containing up to 0.08 volume per

cent fibres. These serrations are probably due to twinning. Serrations

were also found in stage IV of the load elongation curves of the W-Zn com-

posites containing up to 0.08 volume per cent fibres. These serrations are

due to fibre fracture. Serrations due to fibre fractures were found until

the final stages of deformation. Serrations were not seen in the load-

elongation curves of the composites containing more than 0.08 volume per

cent of fibres.

Since the curves for all the specimens tested are not given, the

important physical and tensile properties obtained from the curves of all

the specimens tested are given in Tables 5a and 5b.

The variations in ultimate tensile strengths of W-Zn composites,

σ_{cu}, with volume fractions of the tungsten fibres, $V_f\%$, present are shown

in Figure 15. The ultimate tensile strengths of the pure zinc single crys-

tals, σ_{mu}, are also plotted in this figure as points corresponding to zero

volume per cent.

The yield strengths of the W-Zn composites, σ_{cy}, are plotted

against $V_f\%$ in Figure 16. The yield strengths of pure zinc crystals, σ_{my},

are also plotted in this figure.

Finally, the slope of the second stage, $\dfrac{d\sigma_c}{d\epsilon}$, of the true stress-

true strain curves of W-Zn composites were measured. These values are

plotted against $V_f\%$ in Figure 17.

TABLE 5a

TENSILE PROPERTIES OBTAINED FROM THE TRUE STRESS-STRAIN CURVES OF TUNGSTEN WIRE, ZINC SINGLE CRYSTALS, AND W-Zn COMPOSITES

SP. NO.	NO. OF WIRES	$V_f\%$	YIELD STRESS gms/mm^2	$\dfrac{d\sigma_c}{d\epsilon}$ gms/mm^2	STRESS AT 0.05% OFFSET FROM STAGE II gms/mm^2	U.T.S. gms/mm^2	STRAIN AT U.T.S. %
W-wire	--	100	23×10^4	--	--	36×10^4	2.29
X-6	0	0	62	--	--	3520	104.67
X-7	0	0	59	--	--	3500	116.64
C-7	6	0.023	82	2.8×10^4	240	520	14.44
C-8	6	0.020	63	3.1×10^4	210	1500	57.20
C-16	6	0.018	56	1.2×10^4	190	3400	99.50
C-46	6	0.018	94	9.6×10^3	220	4600	138.03
C-13	12	0.036	67	2.7×10^4	230	1300	51.90
C-14	12	0.037	63	3.0×10^4	280	3800	102.00
C-17	25	0.080	85	2.9×10^4	260	350	2.62
C-18	25	0.081	97	4.0×10^4	390	940	48
C-19	25	0.080	98	4.9×10^4	390	480	1.97
C-23	25	0.076	65	6.3×10^4	460	3200	104.83
C-25	25	0.078	66	7.7×10^4	430	3800	115.24
C-20	100	0.322	100	1.8×10^5	1100	1500	2.25
C-21	100	0.324	110	2.2×10^5	1000	1500	1.53
C-26	100	0.303	100	1.6×10^5	1100	1600	1.63
C-53	100	0.298	64	1.4×10^5	940	1100	1.04

TABLE 5b

TENSILE PROPERTIES OBTAINED FROM THE TRUE STRESS-STRAIN CURVES OF W-Zn COMPOSITES

SP. NO.	NO. OF WIRES	$V_f\%$	YIELD STRESS gms/mm^2	$\dfrac{d\sigma_c}{d\varepsilon}$ gms/mm^2	STRESS AT 0.05% OFFSET FROM STAGE II gms/mm^2	U.T.S. gms/mm^2	STRAIN AT U.T.S. %
C-27	186	0.553	120	3.4×10^5	1700	2600	2.59
C-29	186	0.558	130	2.4×10^5	1700	2300	1.22
C-30	186	0.574	130	3.8×10^5	1600	2400	1.03
C-31	186	0.562	140	3.9×10^5	1800	2300	0.86
C-32	186	0.565	150	3.9×10^5	1700	2500	1.61
C-51	186	0.587	130	2.9×10^5	1900	2400	1.53
C-36	372	1.144	210	7.7×10^5	3500	5200	2.07
C-38	372	1.163	190	8.2×10^5	3700	4800	0.91
C-39	372	1.146	190	8.2×10^5	3300	4700	1.07
C-40	372	1.110	190	6.3×10^5	3300	4800	2.08
C-41	372	1.089	210	7.0×10^5	3600	4800	1.52
C-3	743	2.298	260	1.1×10^6	6300	8900	2.07
C-9	743	2.357	260	1.4×10^6	7000	10400	2.14
C-10	743	2.321	250	1.2×10^6	6800	9700	1.57
C-11	743	2.276	250	1.3×10^6	7000	9100	1.01
C-58	743	2.357	260	1.3×10^6	7400	10000	1.96
C-42	1484	4.568	330	1.9×10^6	13000	19400	2.39
C-55	1486	4.583	330	2.2×10^6	14000	19500	3.26
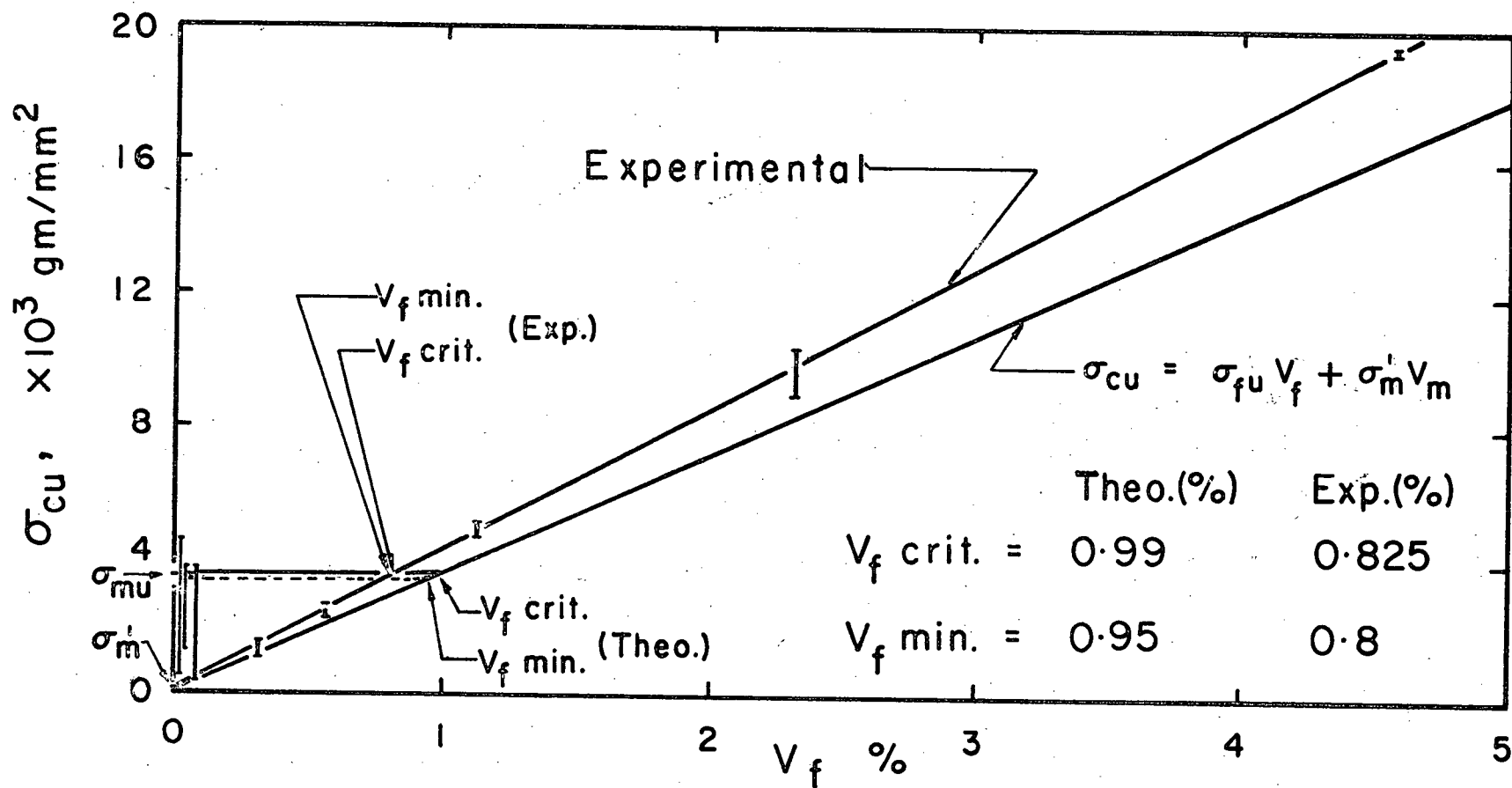
Fig. 15. U.T.S. Vs. $V_f\%$ Plots of W-Zn Composites.
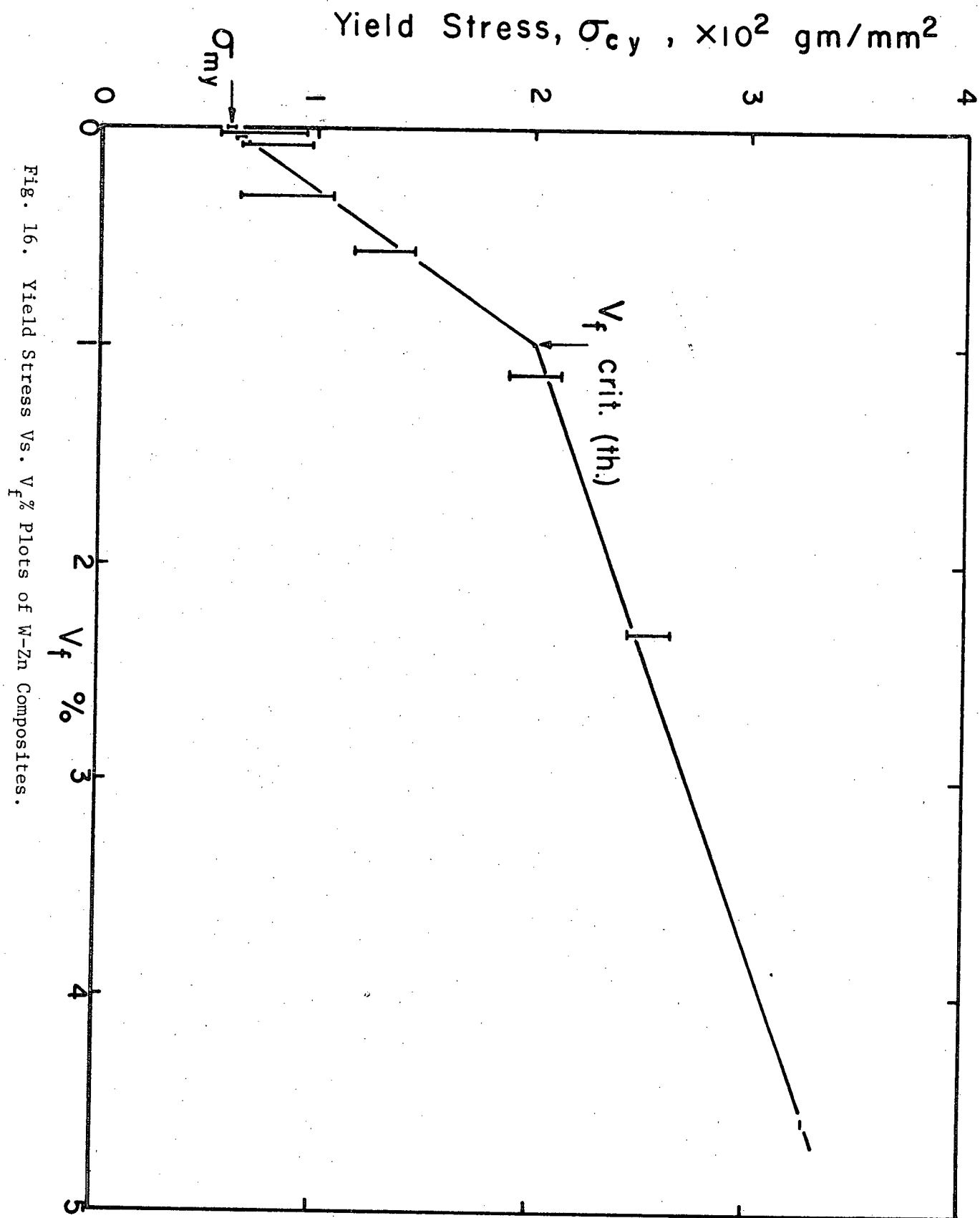
Fig. 16. Yield Stress Vs. V_f% Plots of W-Zn Composites.
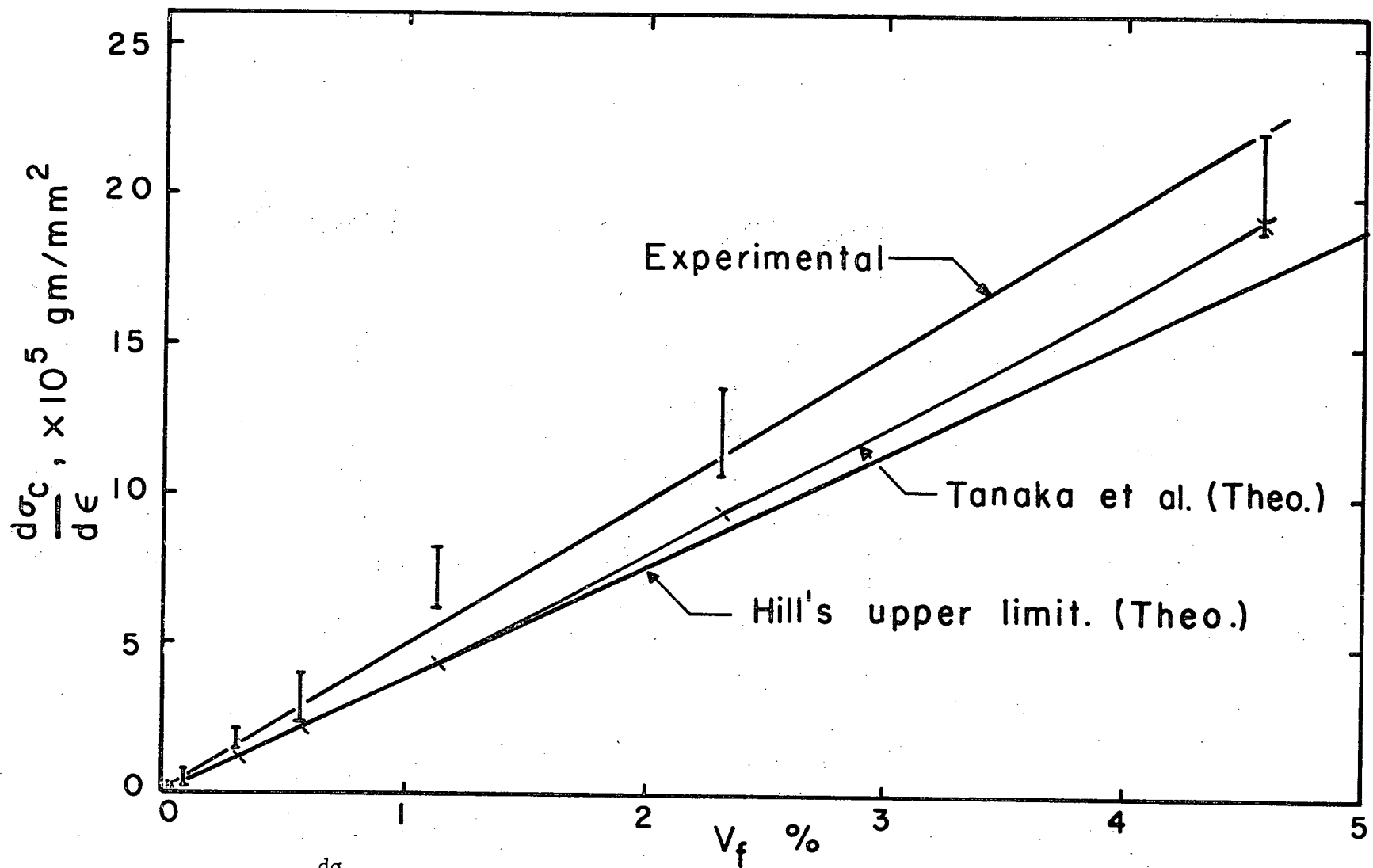
Fig. 17. $\frac{d\sigma_c}{d\epsilon}$ Vs. $V_f\%$ Plots of W-Zn Composites.

48

σ_{cy} and $\dfrac{d\sigma_c}{d\epsilon}$ values are found to increase with increasing value

of $V_f\%$. σ_{cu} values are also found to increase with increasing value of

$V_f\%$ except at lower $V_f\%$. At lower values of $V_f\%$, σ_{cu} values are found to

be constant as $V_f\%$ increases.

B.3. Derived Stress-Strain Curves for the Matrices of the Composites:

In most previous work, expression (4) has been found to be in

good agreement with the experimental values. In the present work it was

not possible to find E_{cI} experimentally and hence to check the agreement

with the expression.

According to expression (3) if there is no interaction between

the fibre and the matrix, the σ_m value should follow the stress-strain

curve of the free matrix. To find the actual stresses in the matrix of

the composites, σ_m'' values were derived from the experimental values of

σ_c, V_f, V_m and σ_f. The relation[11] used is:

$$\sigma_m'' = \frac{\sigma_c}{V_m} - \frac{V_f}{V_m}\sigma_f, \quad V_m + V_f = 1 \tag{23}$$

This involves the assumption that $\epsilon_f = \epsilon_m = \epsilon_c$, and that the stress-strain

curve of the fibres obtained individually, remains the same in the com-

posite. Expression (23) is the same as expression (3) except for σ_m'', where

σ_m'' is the actual stress in the matrix of the composite.

The derived stress-strain curves for the matrices of the composites,

obtained using expression (23) are given in Figure 18. The stress-strain

curve of pure zinc crystals is also given in the same figure.

The derived stress-strain curves of the matrices in the W-Zn com-

posites exhibit linear portions corresponding to stage I and II of the
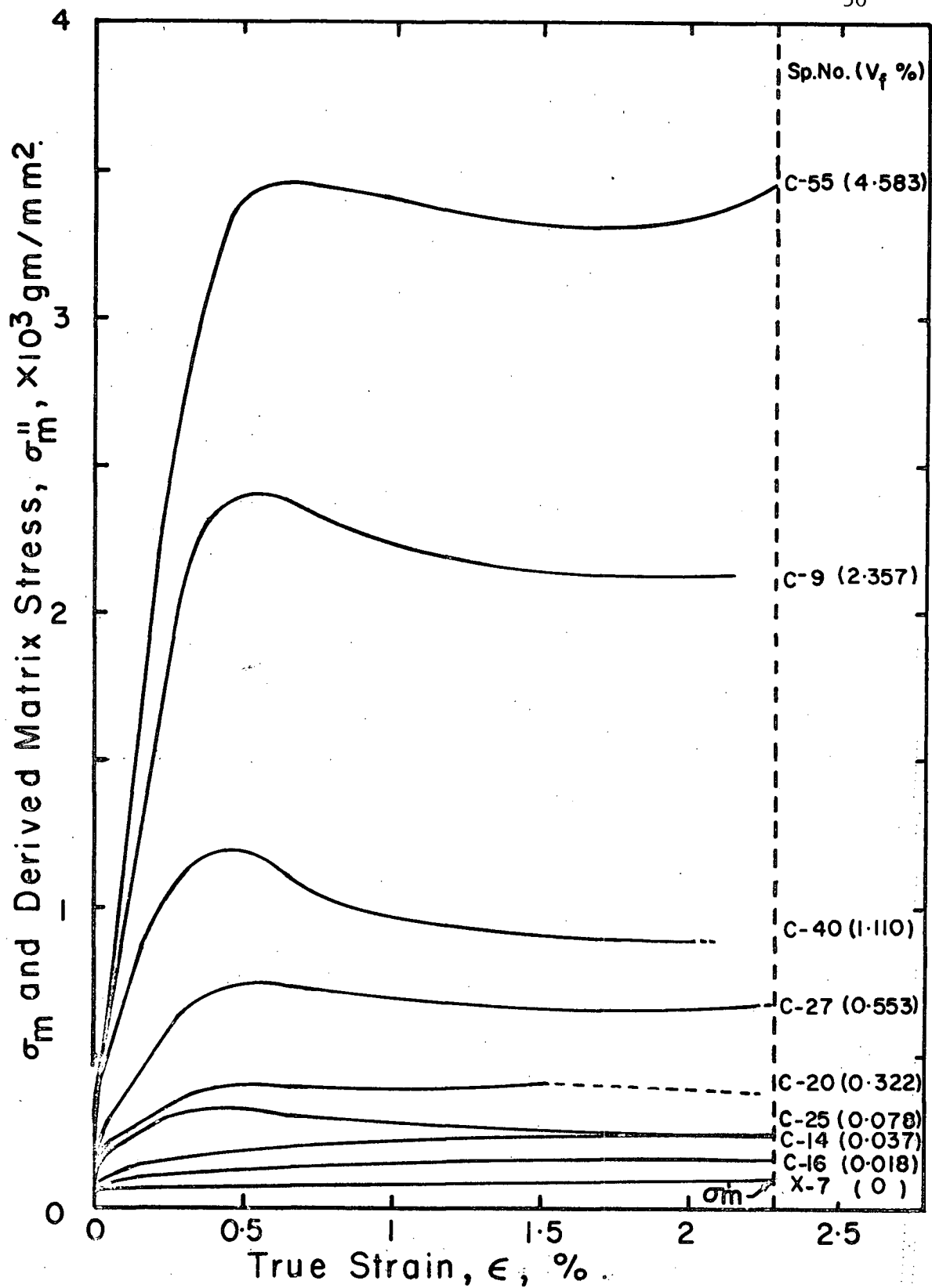
Fig. 18. Derived Matrix Stress-strain Curves of W-Zn Composites
and the True Stress-strain Curve of Zinc Crystal.

stress-strain curves of the W-Zn composites. In expression (5) $\frac{d\sigma_m}{d\epsilon}$ is

the slope of the stress-strain curve of the free matrix at a particular

strain. This is based on the assumption that there is no interaction be-

tween the fibre and the matrix. For the actual matrix of the W-Zn com-

posites the slope $\frac{d\sigma_m''}{d\epsilon}$ corresponding to stage II is obtained using the

relation:

$$\frac{d\sigma_m''}{d\epsilon} = \frac{E_{cII} - E_f V_f}{V_m} \, , \quad V_f + V_m = 1 \tag{24}$$

This assumes that $\epsilon_f = \epsilon_m = \epsilon_c$ and E_f remains the same in the composite.

$\frac{d\sigma_m''}{d\epsilon}$ values were calculated using the experimental values of E_{cII},

E_f, V_f and expression (24). $\frac{d\sigma_m''}{d\epsilon}$ values are plotted against $V_f\%$ in Figure

19.

B.4. Resolved Shear Stress-Shear Strain Curves for Zinc Single Crystal

and Tungsten-Zinc Composites:

When working with single crystals or composites with a single cry-

stal matrix, it is sometimes more appropriate to present the deformation

curves in terms of resolved shear stress-shear strain curves. Kelly and

Nicholson[42] have found that single crystals containing particles of a

hard second phase deform not by slip in a single glide system, but by slip

in many intersecting systems. This leads to a stress-strain curve inde-

pendent of orientation.

In the present work, the matrix of the W-Zn composite was a single

crystal. At room temperature, only one slip plane (0001) is operative in
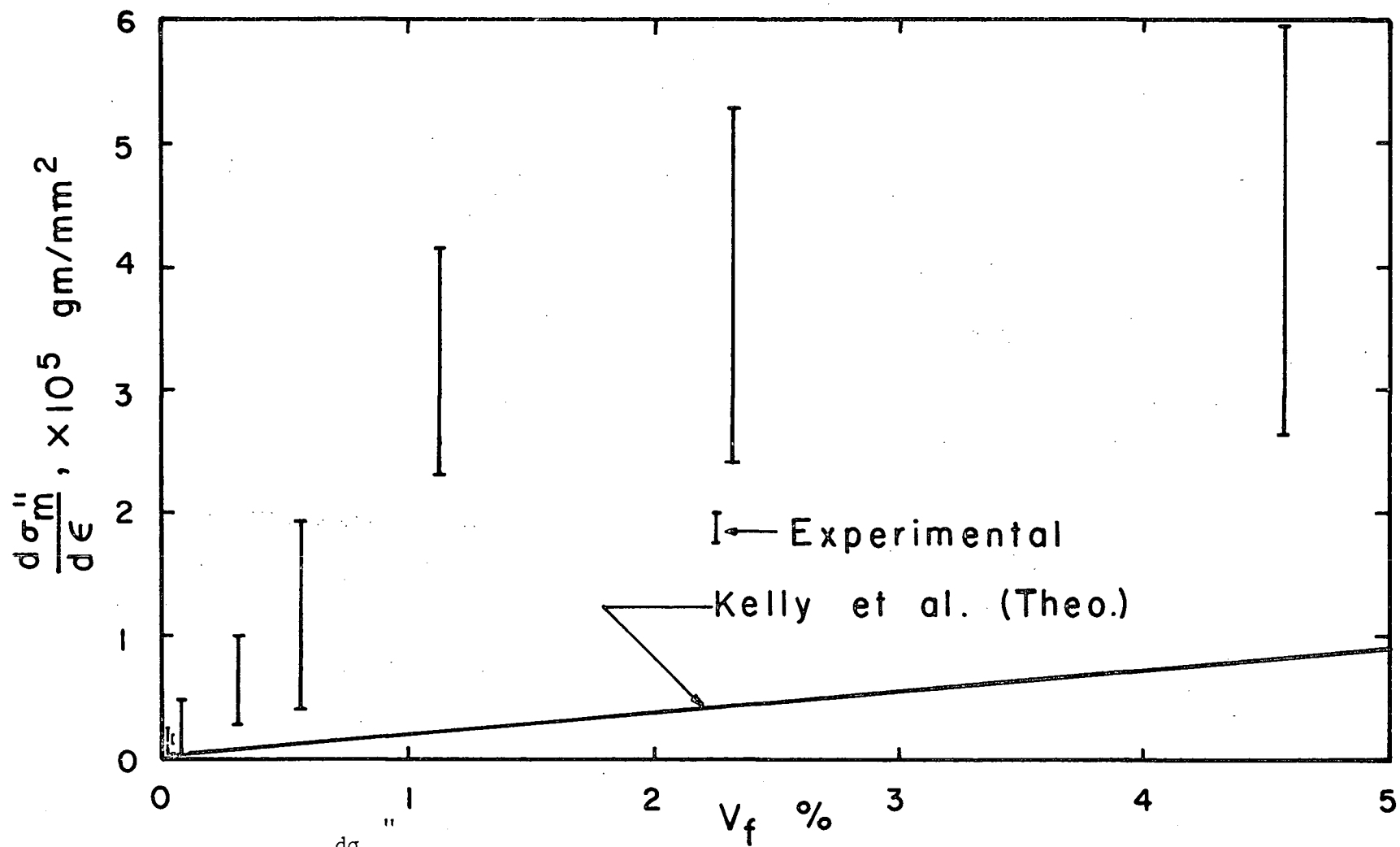
Fig. 19. $\dfrac{d\sigma_m''}{d\epsilon}$ Vs. V_f% Plots of the Matrix of W–Zn Composites.

h.c.p. zinc single crystals at the orientation involved. Hence, it is assumed that the matrix in W-Zn composites deforms by slip on the basal plane (0001). Even though there are three [11$\bar{2}$0] slip directions, the most favourable one is assumed to be operative.

Based on these assumptions, the resolved shear stress-shear strain curves were obtained for W-Zn composites and pure zinc crystals.

The relations[43] used to obtain the resolved shear stress-shear strain curves from the load-elongation curves are:

$$\tau = \frac{P}{A_o} \sin \chi_o \frac{l_o}{l} \sqrt{(\frac{l}{l_o})^2 - \sin^2 \lambda_o} \qquad (25)$$

and

$$\gamma = \frac{1}{\sin \chi_o} (\sqrt{(\frac{l}{l_o})^2 - \sin^2 \lambda_o} - \cos \lambda_o) \qquad (26)$$

P is the tensile load. l is the gauge length after deformation, i.e., at P. A_o and l_o are the initial area of cross section and gauge length respectively. χ_o is the angle between the specimen axis (tensile axis) and slip plane [(0001)]. λ_o is the angle between the specimen axis (tensile axis) and the most favourable slip direction ([11$\bar{2}$0]). τ and γ are resolved shear stress and shear strain respectively.

The resolved shear stress-shear strain curves for some of the specimens are given in Figures 20a and 20b. Similar curves were obtained for the other specimens.

Physical properties, and the important mechanical properties from the resolved shear stress-shear strain curves are given in Tables 6a and 6b.
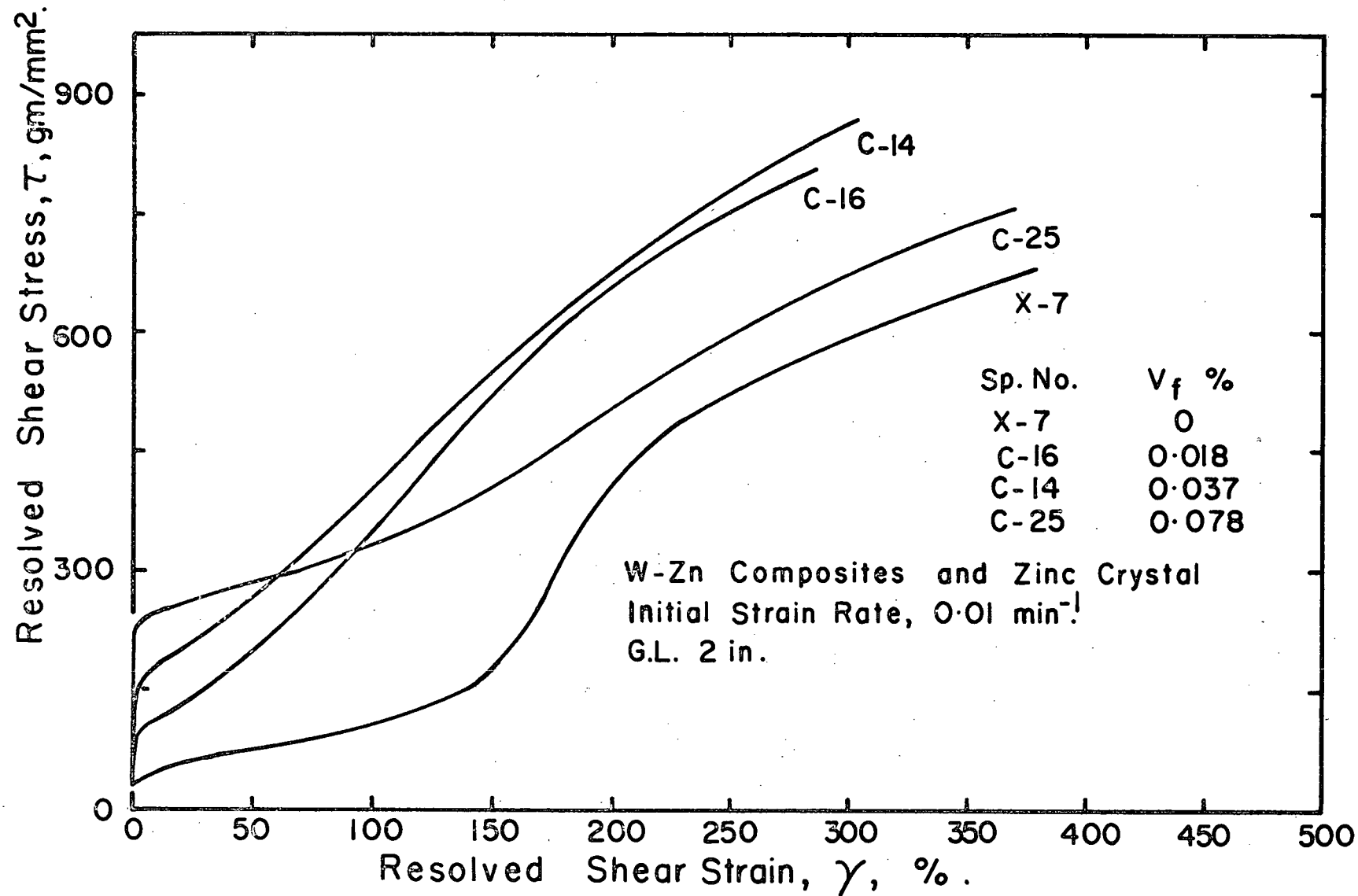
Fig. 20a. Resolved Shear Stress-Shear Strain Curves of a Zinc Crystal and W-Zn Composites.
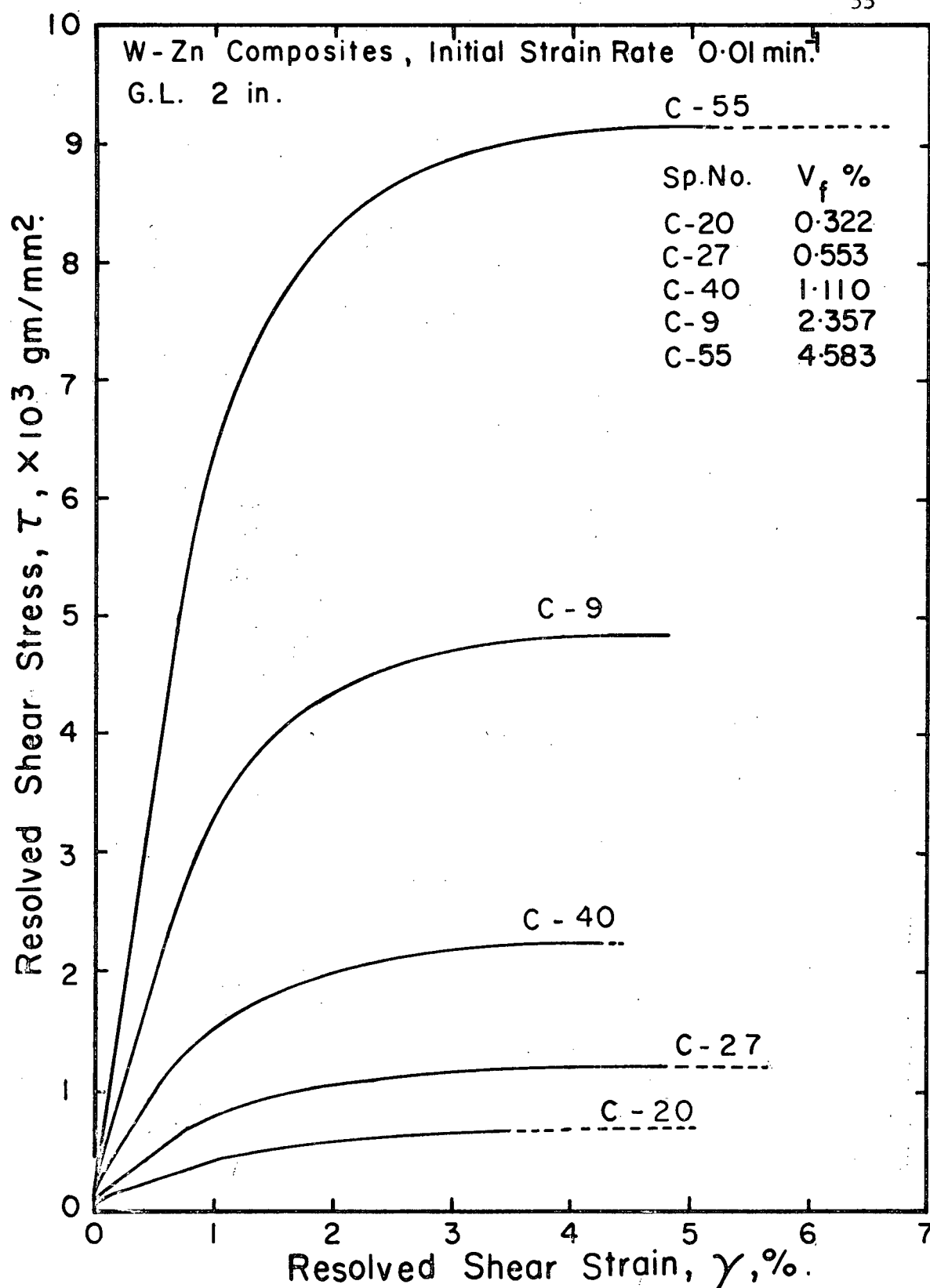
Fig. 20b.   Resolved Shear Stress-Shear Strain Curves of W-Zn
Composites.

TENSILE PROPERTIES OBTAINED FROM THE RESOLVED SHEAR STRESS-SHEAR STRAIN CURVES
OF PURE ZINC CRYSTALS AND W-Zn COMPOSITES

SP. NO.	NO. OF WIRES	AREA OF C/S mm^2	$V_f\%$	χ_o^o	λ_o^o	C.R.S.S. τ_c gms/mm^2	SLOPE OF THE ELASTIC-PLASTIC REGION gms/mm^2	FLOW STRESS AT 0.05% OFFSET FROM ELASTIC-PLASTIC REGION gms/mm^2	MAX. FLOW STRESS gms/mm^2	STRAIN AT MAX. FLOW STRESS %
X-6	0	41.29	0	40	44	31	--	--	770	318
X-7	0	41.60	0	40	47	26	--	--	680	380
C-7	6	22.18	0.023	41	45	38	7.3×10^3	88	230	31
C-8	6	25.99	0.020	40	42	30	6.8×10^3	100	500	140
C-16	6	28.13	0.018	42	46	26	3.3×10^3	73	810	286
C-46	6	28.03	0.018	44	47	45	2.7×10^3	93	800	464
C-13	12	28.51	0.036	41	46	31	5.3×10^3	98	440	126
C-14	12	27.90	0.037	41	47	29	7.3×10^3	110	880	302
C-17	25	26.73	0.080	41	45	39	6.7×10^3	110	160	5.6
C-18	25	26.16	0.081	41	45	45	8.4×10^3	180	340	113
C-19	25	26.74	0.080	41	45	46	10.2×10^3	180	230	4.2
C-23	25	27.88	0.076	40	45	30	12.8×10^3	210	710	320
C-25	25	27.45	0.078	40	45	30	14.9×10^3	200	760	370
C-20	100	26.39	0.322	40	47	45	34.9×10^3	420	670	5.1
C-21	100	26.25	0.324	40	47	47	39.3×10^3	420	660	3.5
C-26	100	28.08	0.303	41	46	46	35.5×10^3	470	710	3.5
C-53	100	28.56	0.298	38	40	30	31.8×10^3	400	520	2.2

TENSILE PROPERTIES OBTAINED FROM THE RESOLVED SHEAR STRESS-SHEAR STRAIN CURVES
OF W-Zn COMPOSITES

SP. NO.	NO. OF WIRES	AREA OF C/S mm^2	$V_f\%$	χ_o°	λ_o°	C.R.S.S. τ_c gms/mm^2	SLOPE OF THE ELASTIC-PLASTIC REGION gms/mm^2	FLOW STRESS AT 0.05% OFFSET FROM ELASTIC-PLASTIC REGION gms/mm^2	MAX. FLOW STRESS gms/mm^2	STRAIN AT MAX. FLOW STRESS %
C-27	186	28.62	0.553	40	45	53	71.7×10^3	790	1200	5.7
C-29	186	28.36	0.558	40	45	58	50.6×10^3	750	1000	2.6
C-30	186	27.57	0.574	42	46	61	78.0×10^3	790	1100	2.2
C-31	186	28.15	0.562	42	46	64	91.8×10^3	750	1100	1.8
C-32	186	28.02	0.565	42	46	68	92.5×10^3	770	1200	3.2
C-51	186	26.99	0.587	38	40	63	59.1×10^3	910	1100	3.2
C-36	372	27.67	1.144	40	42	102	20.9×10^4	1500	2500	4.2
C-38	372	27.23	1.163	40	42	92	21.9×10^4	1600	2300	1.8
C-39	372	27.63	1.146	37	39	88	20.9×10^4	1400	2200	2.2
C-40	372	28.51	1.110	37	39	89	15.2×10^4	1300	2200	4.4
C-41	372	28.55	1.089	37	39	96	16.8×10^4	1500	2200	3.2
C-3	743	27.51	2.298	37	40	122	26.8×10^4	2600	4100	4.3
C-9	743	26.83	2.357	42	46	122	33.5×10^4	3000	4900	4.4
C-10	743	27.24	2.321	40	44	116	28.9×10^4	3000	4500	3.2
C-11	743	27.78	2.276	38	42	112	33.3×10^4	2600	4100	2.0
C-58	743	26.82	2.357	40	44	121	30.0×10^4	3200	4600	4.0
C-42	1484	27.65	4.568	39	40	158	56.4×10^4	5900	9300	4.6
C-55	1486	27.59	4.583	39	40	155	67.7×10^4	5900	9100	6.7

Critical resolved shear stress (C.R.S.S.) τ_c is defined to be the shear stress at which the load-elongation curve first deviates from linearity.

τ_c values are plotted against $V_f\%$ in Figure 21. Also, the slope of the elastic-plastic region is plotted against $V_f\%$ in Figure 22.

The plots were made to see the effects of fibre reinforcement on the work hardening behaviour.
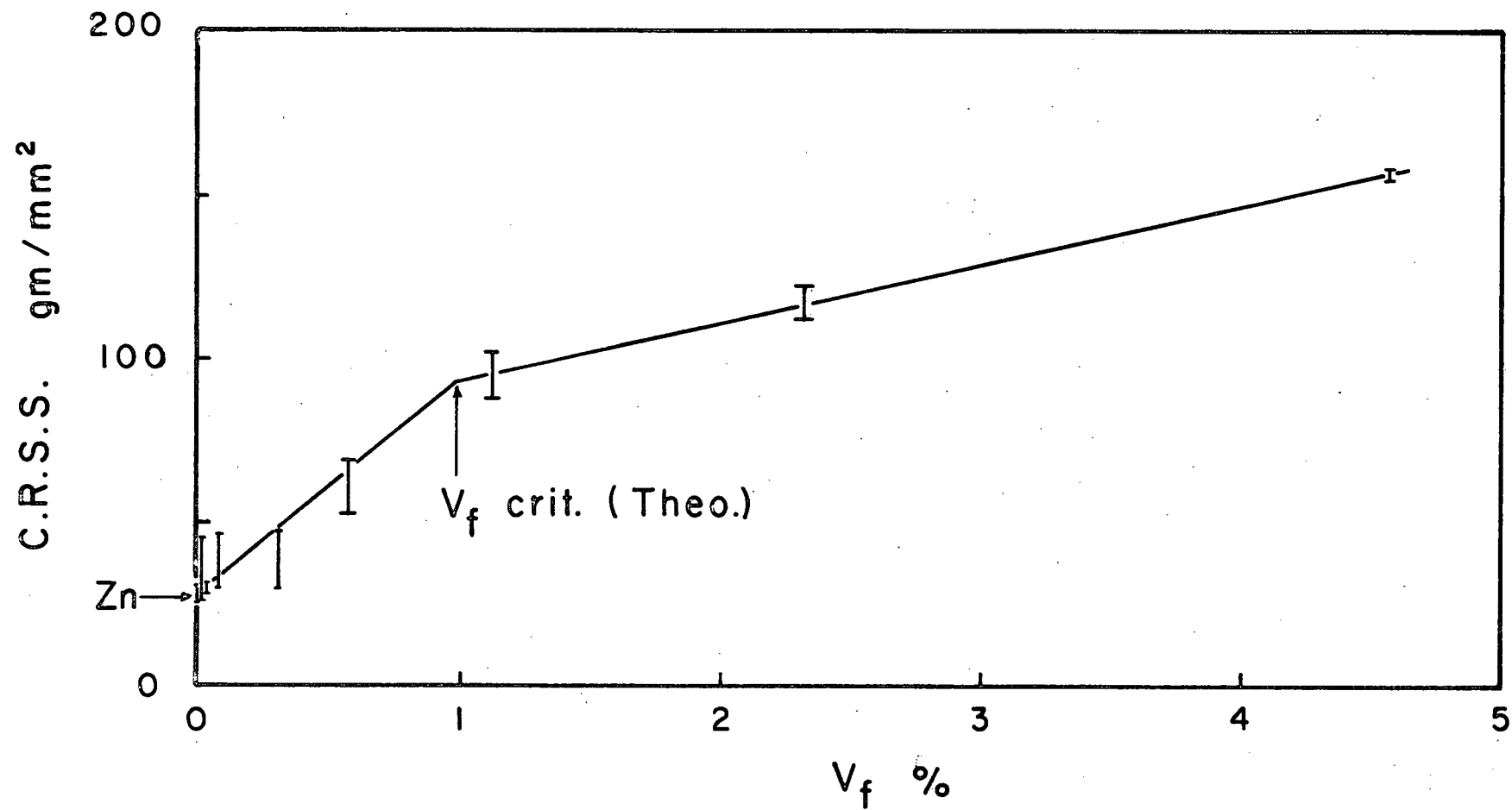
Fig. 21.   C.R.S.S. Vs. V_f% Plots of W-Zn Composites.
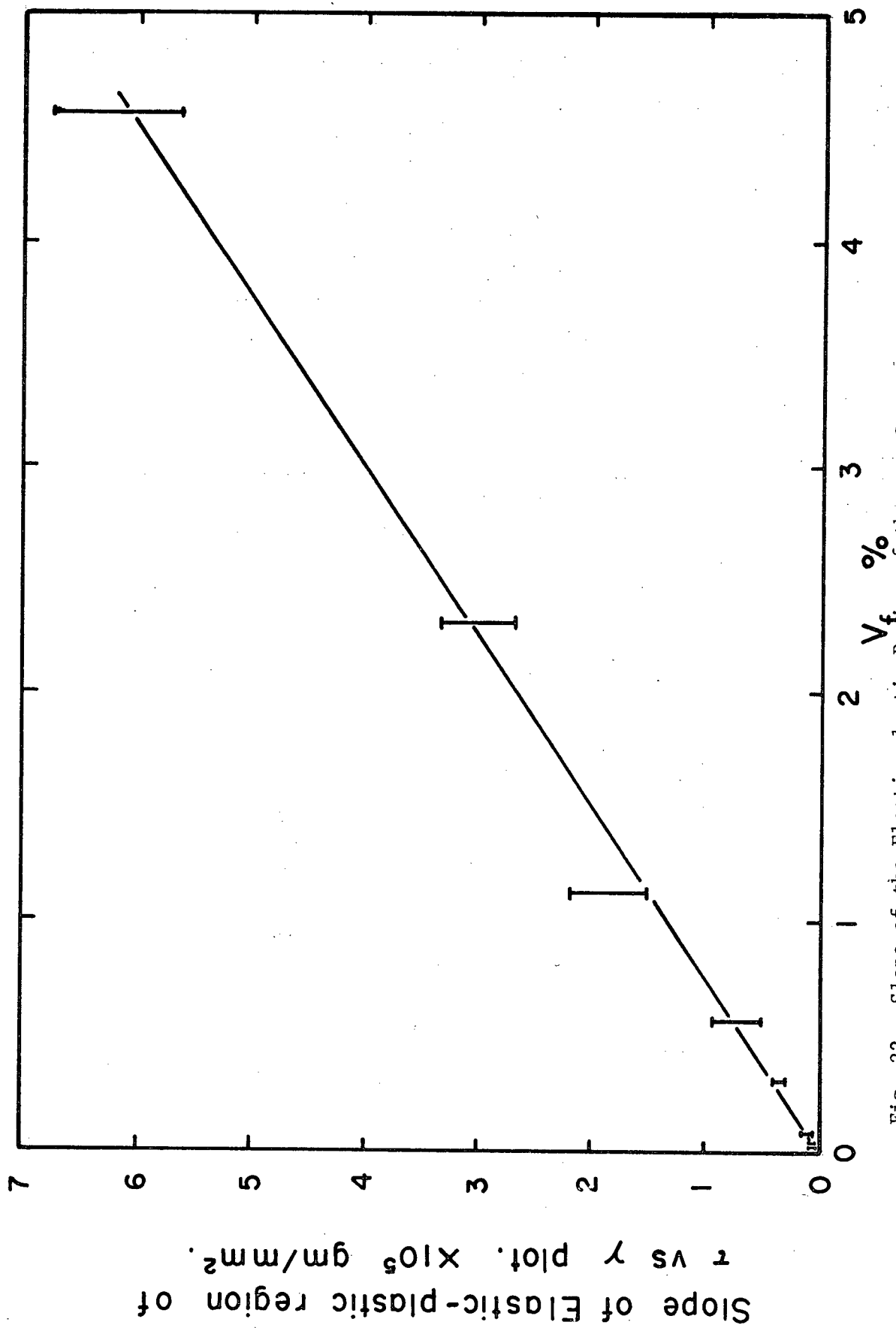
Fig. 22. Slope of the Elastic-plastic Region of the τ-γ Curves Vs. V_f% Plots of W-Zn Composites.

Slope of Elastic-plastic region of
τ vs γ plot. $\times 10^5$ gm/mm^2.

V_f %

IV. DISCUSSION

A. Scatter in the Experimental Results:

The scatter in the stress-strain curves of pure zinc crystals is due to conditions of growth, different impurities present and the low angle boundaries present in the crystal.

The small scatter in the stress-strain curves of tungsten wires is due to the non-uniformity of the surface and residual stresses present in the wires.

The scatter in the stress-strain curves of W-Zn composites, containing the same volume fractions of tungsten fibres, may be due to:

(a) poor bonding between some fibres and the zinc matrix[20]

(b) misorientation of the fibres with the specimen axis[13, 32]

(c) presence of zinc oxide

(d) presence of low angle boundaries in the single crystal matrix of zinc

(e) non uniform distribution of the tungsten fibres in the matrix.

No quantitative measurements are possible to estimate the contributions to the scatter from each one of the above factors.

An estimation of the maximum scatter in the experimental results was made. The estimates are given in Table 7.

TABLE 7

ESTIMATES OF THE SCATTER IN THE EXPERIMENTAL RESULTS

	MEAN $V_f\%$	MEAN VALUE gms/mm^2	PERCENTAGE SCATTER (Maximum)
σ_{cu}	2.316	9700	±8
σ_{cy}	1.126	200	±6
$\dfrac{d\sigma_c}{d\varepsilon}$	4.575	2.05×10^6	±8
σ_{mu}	0	3510	±0.3
$\dfrac{d\sigma_m''}{d\varepsilon}$	4.575	4.3×10^5	±39
C.R.S.S.	1.126	95	±7
Slope of the elastic-plastic region of $\tau-\gamma$ plot	4.575	62×10^4	±9

B. Cause for the Greater Elongation of W-Zn Composites Compared to the

Free Tungsten Wire:

Some of the W-Zn composites tested exhibited elongations greater

than the elongation of a tungsten wire tested separately. The composites

containing a volume fraction of the fibres less than $V_f$min cannot fail

since the ductile zinc matrix supports the load even after the fibres have

fractured. In the present work a value of 0.0095 is obtained for $V_f$min.,

using expression (9).

The extra elongation observed in W-Zn composites containing a

volume fraction of fibres greater than V_f min. is due to multiple necking[44]

of the tungsten wires in the composites. Multiple necking in the fibres

was also observed in W-brass composites.[44] The multiple necking of tungsten

wires in a brass matrix was found to result from local strain hardening

of the brass matrix in the vicinity of each neck enabling the matrix to

control composite deformation locally.

C. Discrepancy Between the Experimental Strengths of W-Zn Composites and

Values Predicted According to "Rule of Mixtures":

(i) In the present work it was assumed that expression (4) holds

good for stage I. Hence, the value of V_f crit. was calculated using ex-

pression (7). The value of V_f crit. is found to be 0.0099. It can be

seen from Figure 16 that yield stress varies linearly with V_f% above and

below V_f crit.

(ii) Excluding stage I of the stress-strain curves of W-Zn com-

posites, the stress-strain curves predicted according to expression (3)

did not agree with the experimentally obtained stress-strain curves for W-Zn composites. The higher values of the stresses found in the experimental curves can be attributed to:

(a) hardening of the matrix due to the different effective Poisson's ratio of the two constituents of the composite,[11,30,45]

(b) hardening of the matrix by dislocation pile-ups caused by blocking of the motion of the dislocations in the matrix by the fibres[11,34]

Hardening due to (a) and (b) can account for stage II deformation. In stage III hardening due to (a) becomes negligibly small since both constituents of the composite deform plastically and Poisson's ratio for each constituent becomes the same. Hence, in stage III hardening in the matrix can only be due to (b). This continues until fracture.

The values of ultimate tensile strengths of W-Zn composite obtained according to expression (2) are found to be lower than the experimental values, (Figure 15, and Tables 8a and 8b). These differences in the predicted values and the experimental values are accounted for by matrix hardening due to dislocation pile ups. Also there may be a small effect due to oxide present.

Figure 15 shows that the value of V_f crit. predicted (0.99%) according to expression (7) is higher than the experimental value of V_f crit. (0.825%). This also can be accounted for by matrix hardening.

The extent of matrix hardening depends on the volume fraction of the tungsten fibres present in the matrix. This can be seen from Figure 18 in

TABLE 8a

COMPARISON OF THE EXPERIMENTAL AND THEORETICAL VALUES
(W–Zn Composites)

SP. NO.	V_f%	$\frac{d\sigma_c}{d\epsilon}$ Exp. gms/mm^2	$\frac{d\sigma_c}{d\epsilon}$ Theo. Eqn. (33) gms/mm^2	$\frac{d\sigma_c}{d\epsilon}$ Theo. Eqn. (39) gms/mm^2	U.T.S. Exp. gms/mm^2	U.T.S. Theo. Eqn. (2) gms/mm^2	$\frac{d\sigma_m''}{d\epsilon}$ Exp. gms/mm^2	$\frac{d\sigma_m''}{d\epsilon}$ Theo. Eqn. (40) gms/mm^2
X-6	0	--	--	--	3520	$\sigma_{m_1} = 88$	--	--
X-7	0	--	--	--	3500	$\sigma_m = 88$	--	--
C-7	0.023	2.8×10^4	8.7×10^3	8.4×10^3	520	170	2.0×10^4	4.3×10^2
C-8	0.020	3.1×10^4	7.4×10^3	7.2×10^3	1500	160	2.4×10^4	3.7×10^2
C-16	0.018	1.2×10^4	6.9×10^3	6.64×10^3	3400	150	5.5×10^3	3.4×10^2
C-46	0.018	9.6×10^3	6.9×10^3	6.66×10^3	4600	150	3.1×10^3	3.4×10^2
C-13	0.036	2.7×10^4	1.4×10^4	1.3×10^4	1300	220	1.4×10^4	6.7×10^2
C-14	0.037	3.0×10^4	1.4×10^4	1.3×10^4	3800	220	1.7×10^4	6.9×10^2
C-17	0.080	2.9×10^4	3.0×10^4	2.9×10^4	350	370	4.4×10^2	1.5×10^3
C-18	0.081	4.0×10^4	3.1×10^4	3.0×10^4	940	380	1.1×10^4	1.5×10^3
C-19	0.080	4.9×10^4	3.0×10^4	2.9×10^4	480	370	2.1×10^4	1.5×10^3
C-23	0.076	6.3×10^4	2.9×10^4	2.8×10^4	3200	360	3.6×10^4	1.4×10^3
C-25	0.078	7.7×10^4	2.9×10^4	2.8×10^4	3800	370	4.9×10^4	1.5×10^3
C-20	0.322	1.8×10^5	1.2×10^5	1.2×10^5	1500	1200	6.8×10^4	6.0×10^3
C-21	0.324	2.2×10^5	1.2×10^5	1.2×10^5	1500	1200	1.0×10^4	6.1×10^3
C-26	0.303	1.6×10^5	1.1×10^5	1.1×10^5	1600	1200	5.2×10^4	5.7×10^3
C-53	0.298	1.4×10^5	1.1×10^5	1.1×10^5	1100	1200	3.2×10^4	5.6×10^3

TABLE 8b

COMPARISON OF THE EXPERIMENTAL AND THEORETICAL VALUES
(W-Zn Composites)

SP. NO.	V_f%	$\frac{d\sigma_c}{d\epsilon}$ Exp. gms/mm²	$\frac{d\sigma_c}{d\epsilon}$ Theo. Eqn. (33) gms/mm²	$\frac{d\sigma_c}{d\epsilon}$ Theo. Eqn. (39) gms/mm²	U.T.S. Exp. gms/mm²	U.T.S. Theo. Eqn. (2) gms/mm²	$\frac{d\sigma_m}{d\epsilon}''$ Exp. gms/mm²	$\frac{d\sigma_m}{d\epsilon}''$ Theo. Eqn. (40) gms/mm²
C-27	0.553	3.4×10^5	2.1×10^5	2.1×10^5	2600	2100	1.4×10^5	1.0×10^4
C-28	0.558	2.4×10^5	2.1×10^5	2.1×10^5	2300	2100	3.9×10^4	1.0×10^4
C-30	0.574	3.8×10^5	2.2×10^5	2.1×10^5	2400	2100	1.7×10^5	1.1×10^4
C-31	0.562	3.9×10^5	2.1×10^5	2.1×10^5	2300	2100	1.9×10^5	1.1×10^4
C-32	0.565	3.9×10^5	2.1×10^5	2.1×10^5	2500	2100	1.9×10^5	1.1×10^4
C-51	0.587	2.9×10^5	2.2×10^5	2.2×10^5	2400	2200	8.1×10^4	1.1×10^4
C-36	1.144	7.7×10^5	4.3×10^5	4.4×10^5	5200	4200	3.7×10^5	2.1×10^4
C-38	1.163	8.2×10^5	4.4×10^5	4.4×10^5	4800	4200	4.1×10^5	2.2×10^4
C-39	1.146	8.2×10^5	4.3×10^5	4.4×10^5	4700	4200	4.2×10^5	2.1×10^4
C-40	1.110	6.3×10^5	4.2×10^5	4.2×10^5	4800	4100	2.3×10^5	2.1×10^4
C-41	1.089	7.0×10^5	4.1×10^5	4.1×10^5	4800	4000	3.1×10^5	2.0×10^4
C-3	2.298	1.1×10^6	8.7×10^5	9.1×10^5	8900	8300	2.4×10^5	4.2×10^4
C-9	2.357	1.4×10^6	8.9×10^5	9.3×10^5	10400	8500	5.3×10^5	4.3×10^4
C-10	2.321	1.2×10^6	8.8×10^5	9.2×10^5	9700	8400	3.7×10^5	4.2×10^4
C-11	2.276	1.3×10^6	8.6×10^5	9.0×10^5	9100	8200	4.8×10^5	4.2×10^4
C-58	2.357	1.3×10^6	8.9×10^5	9.3×10^5	10000	8500	2.7×10^5	4.3×10^4
C-42	4.568	1.9×10^6	1.7×10^6	1.9×10^6	19400	16400	2.7×10^5	8.1×10^4
C-55	4.583	2.2×10^6	1.7×10^6	1.9×10^6	19500	16400	6.0×10^5	8.1×10^4
W-fibre	100	--	--	--	3.6×10^5	3.6×10^5	--	--

which the derived matrix stress-strain curves do not follow the stress-strain curve of the pure zinc crystal.

D. Stage II of the Stress-Strain Curves of W-Zn Composites:

Hill[30] gave an upper and lower bound for the slope of the second stage of a composite. Tanaka et al.[45] predicted the slope of the second stage and this was found to be in good agreement with the experimental results of Kelly et al.[11] The theoretical and the experimental values are compared and discussed.

(a) Hill:[30]

In Hill's derivation, a single fibre with circular section embedded in a matching circular cylindrical shell of matrix was considered as a rudimentary composite. It was supposed that the composite cylinder was subjected to uniform lateral pressure P and to axial mean tension T acting through rigid constraints keeping the ends plane.

By stress analysis and by frequent use of "law of mixtures," Hill derived an expression which is given by:

$$E_{cI} - V_f E_f - V_m E_m = \frac{4 V_f V_m (\nu_f - \nu_m)^2}{(\frac{V_f}{k_{mp}} + \frac{V_m}{k_{fp}} + \frac{1}{G_m})} \tag{27}$$

where k_{mp} and k_{fp} are the plane strain bulk moduli for lateral dilatation, without longitudinal extension, of the matrix and the fibre respectively.

Hill obtained the bounds on E_{cI} using elastic extremum principles of potential energy and Reuss and Voigt estimates:[46]

The Voigt treatment of reinforcement assumes that the strain throughout the mixture is uniform. Hence he gave an expression,

$$E_V = V_f E_f + V_m E_m \tag{28}$$

for a polycrystal mixture, where E_V is the overall Young's modulus of the mixture and E_m is the Young's modulus of the polycrystalline matrix.

Reuss, also for a polycrystal mixture, assumed that the stress is uniform throughout the matrix and gave the expression,

$$\frac{1}{E_R} = \frac{V_f}{E_f} + \frac{V_m}{E_m} \tag{29}$$

where E_R is the overall modulus of the mixture.

Neither assumption is correct: the Voigt stresses are such that the tractions at phase boundaries would not be in equilibrium, while the implied Reuss strains are such that inclusions (fibres) and matrix could not remain bonded.

From these two estimates it is shown that

$$E_R \leq [E = V_f E_f + V_m E_m] \leq E_V \tag{30}$$

The equality is only valid when $\nu_f = \nu_m$.

On the basis of similar arguments Hill obtained bounds on the plane strain bulk modulus, k_c, of the composite for different transverse rigidities of the fibre and matrix. This in turn gives the bounds for E_{cI}, for elastic behaviour of the compound cylinder, as:

$$\frac{4 V_f V_m (\nu_f - \nu_m)^2}{(\frac{V_f}{k_{mp}} + \frac{V_m}{k_{fp}} + \frac{1}{G_m})} \leq E_{cI} - V_f E_f - V_m E_m \leq \frac{4 V_f V_m (\nu_f - \nu_m)^2}{(\frac{V_f}{k_{mp}} + \frac{V_m}{k_{fp}} + \frac{1}{G_f})} \tag{31}$$

for $G_f \geq G_m$, where G_f and G_m are the rigidity moduli of the fibre and the matrix respectively.

k_{mp} and k_{fp} are the plane strain bulk moduli of fibre and matrix respectively. These bounds are derived for the composite when matrix and fibre are both elastic.

For inelastic behaviour, i.e., when the weaker phase (matrix) does not harden and the stronger phase (fibre) remains linearly elastic, ν_m becomes equal to $\frac{1}{2}$. k_{mp} becomes K_m and E_{cI} becomes the slope of the elastic-plastic region (stage II) $\frac{d\sigma_c}{d\varepsilon}$. $\frac{d\sigma_c}{d\varepsilon}$ can also be denoted by E_{cII}.

Hill obtained an expression for $\frac{d\sigma_c}{d\varepsilon}$ of the elastic-plastic (inelastic) region of the composite. The expression is:

$$\frac{d\sigma_c}{d\varepsilon} = V_f E_f + \frac{V_f V_m (1 - 2\nu_f)^2}{\dfrac{V_f}{K_m} + \dfrac{V_m}{k_{fp}} + \dfrac{1}{G_m}} \tag{32}$$

The bounds on $\frac{d\sigma_c}{d\varepsilon}$ were also derived and are given by:

$$\frac{V_f V_m (1 - 2\nu_f)^2}{\dfrac{V_f}{K_m} + \dfrac{V_m}{k_{fp}} + \dfrac{1}{G_m}} \leq \frac{d\sigma_c}{d\varepsilon} - V_f E_f \leq \frac{V_f V_m (1 - 2\nu_f)^2}{\dfrac{V_f}{K_m} + \dfrac{V_m}{k_{fp}} + \dfrac{1}{G_f}} \tag{33}$$

for $G_f \geq G_m$, also $V_m + V_f = 1$.

$\frac{d\sigma_c}{d\varepsilon}$ values calculated for W-Zn composites using the equality at Hill's upper bound in expression (33) are plotted in Figure 17. The experimental values of $\frac{d\sigma_c}{d\varepsilon}$ obtained for W-Zn composites are higher than the values

predicted (Tables 8a and 8b).

This discrepancy is accounted for by the assumptions made in deriving the expression (33). Expression (33) is derived on the basis of different contractions of the two phases and gradual work hardening of the matrix.

Experimental results show that matrix hardening is not gradual in the composite. Also, lateral constraint is not the only reason for work hardening of the matrix material. There is also hardening due to dislocation pile ups in the matrix.

(b) Tanaka et al.:[45]

Tanaka et al. predicted the slope of the second stage of a composite stress-strain curve. Their prediction was essentially in good agreement with the experimental values of Kelly et al.[11] Their prediction was also checked in the present work.

Tanaka et al. assumed that the matrix deforms plastically and that dislocations are present in contact with the interfaces. Homogeneous plastic deformation takes place by the operation of several slip systems. An expression was developed for the Gibb's free energy of a fibre-reinforced composite as a function of a plastic strain of the matrix.

Thermodynamic stability led to an equilibrium relation between the applied stress σ_c and the plastic strain in the matrix ε_p. The linear relation is given[33] by:

$$\sigma_c = \frac{\sigma_o}{(1 - BV_f)} + \frac{AE_m V_f \varepsilon_p}{(1 - BV_f)} \tag{34}$$

where σ_o is the yield stress of the composite,

$$A = \frac{3(1 - 2\nu_f)E_m + 2(1 + \nu_m)E_f}{(1 + \nu_f)(1 - 2\nu_f)E_m + (1 + \nu_m)E_f} \; (\frac{E_f}{2E_m}) \qquad (35)$$

$$B = \frac{(1 - 2\nu_f)E_m + E_f}{(1 + \nu_f)(1 - 2\nu_f)E_m + (1 + \nu_m)E_f} \; (1 + \nu_m)(\frac{E_f}{E_m}) \qquad (36)$$

where A is a coefficient connected with the elastic energy change. B is a coefficient connected with the external potential energy change.

In a tensile test the recorded total strain ε is the sum of the elastic strain and the plastic strain. For a composite ε is given by:

$$\varepsilon = \varepsilon_p(1 - B_f) + \frac{\sigma_c}{E_c} \qquad (37)$$

E_c is the overall Young's modulus of the composite (same as E_{cI}). From expressions (34) and (37), the measured rate of hardening in stage II is given by:

$$\frac{d\sigma_c}{d\varepsilon} = \frac{A \; V_f E_m}{[(1 - BV_f)^2 + \frac{AV_f E_m}{E_c}]} \qquad (38)$$

Expression (34) was derived on the assumption that low volume fractions of the fibres were present in the composite and that the stress field of any fibre did not interact with that of another. This involves ignoring the disturbance of the internal stress around a fibre by another fibre, which should affect not only the elastic energy but also the interaction energy with applied stress. The effect of the disturbance of the internal stress by other fibres is considered on the assumption that a fibre is surrounded by a phase which has elastic constants determined by the overall elastic constants of the composite.

Hence the hardening rate for a general volume fraction is given by:

$$\frac{d\sigma_c}{d\epsilon} = \frac{A_c V_f E_c}{[(1 - B_c V_f)^2 + A_c V_f]} \tag{39}$$

where A_c and B_c are calculated from A and B replacing [expressions (35) and (36)] E_m and ν_m by E_c and ν_c respectively. As a crude approximation E_c and ν_c can be obtained by the "rule of mixtures."

$\frac{d\sigma_c}{d\epsilon}$ values were calculated using expression (39). Calculated values are plotted in Figure 17. Also, calculated values are compared with the experimental values in Tables 8a and 8b. The experimental values are higher than the predicted values of $\frac{d\sigma_c}{d\epsilon}$.

The composite containing 4.5 volume per cent of fibres was found to give a slope which agreed with the predicted value within the limits of experimental scatter. This may be due to mere coincidence, or the prediction may be in good agreement with the experimental values of W-Zn composites containing more than 4.5 volume per cent of fibres. It is also worth mentioning that Tanaka's predictions did not agree with experimental values obtained for W-Cu composites containing less than 10 volume per cent fibres. Predicted values were lower than the experimental values of W-Cu composites.

In the present work disagreement can be accounted for by inhomogeneous deformation, and by work hardening of the matrix due to dislocation pile ups.

E. Stage II of the Derived Stress-Strain Curves of the Matrix Correspond-

ing to the Second Stage of the Composite Stress-Strain Curve:

Kelly[11] tried to explain the work hardening behaviour of the

matrix especially in the second stage of the composite. In his work on

W-Cu composites, stress-strain curves for the matrix were derived from

the composite stress-strain curves. The slope of the second stage, $\frac{d\sigma_m}{d\epsilon}$

of the derived stress-strain curve was predicted and compared. The pre-

diection was made on the basis of different lateral constraints of the

constituents of the composite.

Neumann et al.[34] predicted $\frac{d\sigma_m}{d\epsilon}$ on the basis of dislocation

pile ups and hence predicted a value for the slip band spacing for W-Cu

composites.

The predictions of Kelly et al.[11] and Neumann et al.[34] are con-

sidered in the present work.

(a) Kelly et al.[11]:

The expressions given for the Young's

moduli E_{cI} and E_{cII} on the basis of the rule of mixtures, and on the assump-

tion of equal strains are true only if the Poisson's ratios are equal, i.e.,

$\nu_f = \nu_m$. When they differ, a lateral stress arises which is proportional to

$|\nu_m - \nu_f|^2$. When fibre and matrix are elastic the value of $|\nu_m - \nu_f|^2$ is

small and hence the effect of lateral stress on E_{cI} is small. When the

matrix yields plastically, the effective ν_m becomes 0.5 since there is

little work hardening, and the value of $|\nu_m - \nu_f|^2$ becomes much larger.

This may affect the stress-strain curves of composites.

Kelly et al., following Hill's ideas and Love's[47] solution of the

problem of a tube under internal pressure, tried to explain the effect of

lateral constraints and derived an expression for the slope of the second

linear portion of the derived stress-strain curve of the matrix correspond-

ing to stage II of the composite.

The model used was a composite cylinder, similar to that of Hill,

with a stiffer phase surrounding the weaker phase. Considering the weaker

phase to be a fluid with Poisson's ratio 0.5 and the bulk modulus of the

matrix, and the stiffer phase to have the elastic properties of the rein-

forcing material, he derived the expression for $\frac{d\sigma_m}{d\epsilon}$ which is given by:

$$\frac{d\sigma_m{}''}{d\epsilon} = \frac{V_f(1 - 2\nu_f)^2}{\frac{V_f}{K_m} + \frac{V_m}{k_{fp}} + \frac{1}{G_f}} \;, \quad V_f + V_m = 1 \tag{40}$$

This expression is the same as that of Hill for $\frac{d\sigma_c}{d\epsilon}$.

The $\frac{d\sigma_m{}''}{d\epsilon}$ values calculated for tungsten-zinc composites using the

above expression are plotted against V_f in Figure 19, and are tabulated in

Tables 8a and 8b. The calculated values of $\frac{d\sigma_m{}''}{d\epsilon}$ are lower than the experi-

mental values, even though the predicted values give an upper limit to the

slopes.

This sort of discrepancy was also observed by Kelly et al.[11] and by

Stuhrke.[48] Kelly et al. gave an explanation for the discrepancy by suggest-

ing that the matrix does not yield completely; i.e., a portion of the matrix

remains elastic during the second stage. But no experimental evidence for

this sort of behaviour is reported. This seems to be unrealistic because

the matrix cannot remain elastic when higher stresses are involved. Predicted

values of $\frac{d\sigma_m{}''}{d\epsilon}$ show that difference in the lateral constraints of the con-

stituents is not the only cause for matrix hardening. The other contribution

may be due to dislocation pile ups.

The presence of dislocation pile ups can be qualitatively supported:

(a) Dislocation pile ups in the matrix would produce stress concentrations in the fibres, and hence fibres would appear weaker in the composite than when tested individually. This is obvious since most of the composite specimens fractured at lower elongations than that of the fibres tested individually (Tables 5a and 5b).

(b) The large stresses in the matrix decrease as soon as the yield strain of the fibres tested alone is reached. This can also be seen in Figure 18.

(c) The large stresses in the matrix should cause yielding of the fibres at a lower strain than when tested individually. It can be seen from Figure 14b that all the composites have yielded in stage II at strains lower than that of the fibre tested individually.

Pinnel et al.[12] made observations on stainless steel-Al composites using transmission electron microscopy. Specimens deformed to strain levels $\leq 8 \times 10^{-3}$ showed that the matrix deformed uniformly and the dislocation densities and configurations were independent of distance from the matrix-fibre interface. Operation of multiple slip systems may be the reason for the absence of dislocation pile ups.

(b) Neumann et al.[34]:

Neumann et al. explained the work-hardening rate observed for the matrix by Kelly et al.[11] on the basis of a system of parallel dislocation pile ups between the fibres. A cylindrical specimen

with axial fibres was considered. The fibre direction was the y-direction. The assumed dislocation model is shown in Figure 23. Under tension in the y-direction edge dislocations infinitely long in the z-direction pile up on slip planes of spacing D_y against boundaries at $x = \pm \frac{a}{2}$, where a is the fibre spacing.

Read[49] calculated $\tau_{\overline{xy}}$ in the coordinate system $(\overline{x}, \overline{y})$, for an infinite row of dislocations spaced at regular intervals. When the dislocation wall is at $x = 0$ the $\tau_{\overline{xy}}$ value is given by:

$$\tau_{\overline{xy}} (\overline{x}, \overline{y} = 0) = \frac{Gb}{2\sqrt{2}(1-\nu)D_y} \ Re \ \{\frac{\overline{x}/d}{Sin^2(\frac{\overline{x}}{d})} - i \ ctg \ \frac{\overline{x}}{d}\} \equiv \frac{b}{D_y} \ \overline{\tau} \ (\frac{\overline{x}}{D_y}) \tag{41}$$

where $d = \frac{D_y(1 + i)}{\Pi \sqrt{2}}$; G, b and ν are the shear modulus, Burgers vector and Poisson's ratio of the matrix respectively; Re is the real part of the function inside brackets; and $\overline{\tau}(\frac{\overline{x}}{D_y})$ is a function of $\frac{\overline{x}}{D_y}$.

A continuous distribution of dislocation walls was considered. Then the sum of the Burgers vector of all the dislocations that lie on the slip planes between the positions $\overline{x}$ and $\overline{x} + d\overline{x}$ is $[b \ D(\overline{x})d\overline{x}]$. $D(\overline{x})$ is a distribution function of $\overline{x}$. The shear stress on the slip plane at a point $\overline{x}' = \overline{x}$ with $\overline{y} = 0$ is:

$$\tau^i (\overline{x}, \overline{y} = 0) = \int_{-\frac{a}{\sqrt{2}}}^{\frac{a}{\sqrt{2}}} D(\overline{x}') \ \frac{b}{D_y} \ \overline{\tau} \ (\frac{\overline{x} - \overline{x}'}{D_y}) \ d\overline{x}' \tag{42}$$

$\tau^i(\overline{x}, o)$ is the shear stress in the interval $\frac{-a}{\sqrt{2}}$ and $\frac{a}{\sqrt{2}}$. In equilibrium the total stress $\tau^i(\overline{x}, o) + \frac{\sigma_a}{2} = 0$ for all $|\overline{x}| \leq \frac{a}{\sqrt{2}}$. σ_a is the applied tensile stress in the matrix in the y-direction.
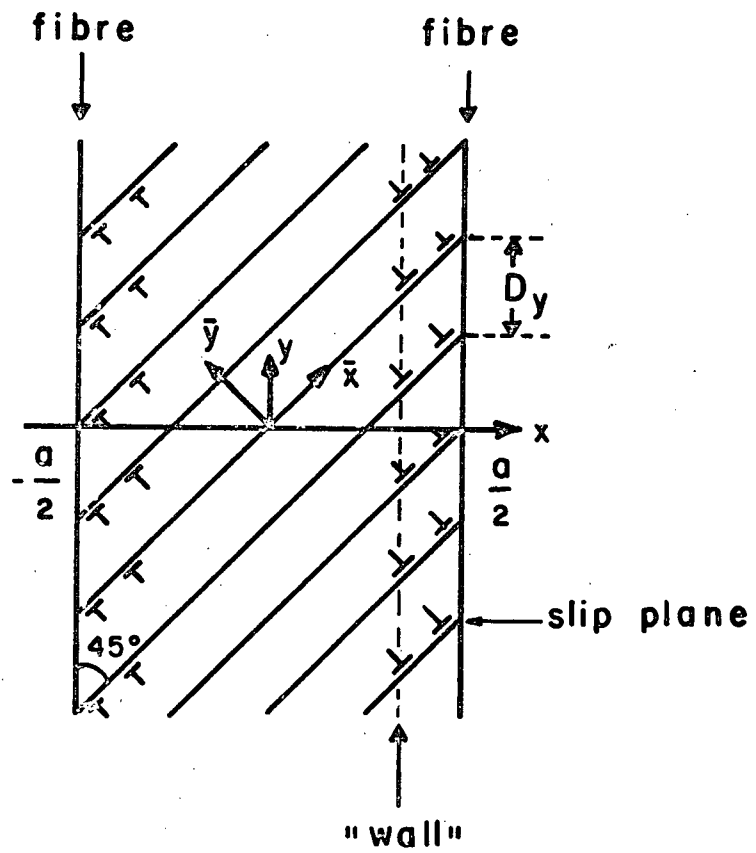
Fig. 23. Dislocation Pile-up Model.

The average plastic strain $\bar{\varepsilon}_p$ in the y direction for $|x| < \frac{a}{2}$ due to the formation of the pile ups is given by:

$$\bar{\varepsilon}_p = \frac{b}{2aD_y} \int_{-\frac{a}{\sqrt{2}}}^{\frac{a}{\sqrt{2}}} \bar{x}' \, D(\bar{x}') \, d\bar{x}' \tag{43}$$

An investigation of the properties of $\tau^i(\bar{x}, o)$ and $\bar{\varepsilon}_p$ leads to the following expression:

$$\bar{\varepsilon}_p = \sigma_a \cdot f\left(\frac{a}{D_y}\right) \tag{44}$$

where $f\left(\frac{a}{D_y}\right)$ is a function of $\frac{a}{D_y}$, and can be obtained by numerical computation of the integral expression for $\bar{\varepsilon}_p$.

However $\bar{\varepsilon}_p$ was approximated analytically using the case of an isolated pile up given by Leibfried.[50] For $D_y \gg a$, $\bar{\varepsilon}_p$ is given by:

$$\bar{\varepsilon}_p = \frac{\Pi}{4} \frac{a}{D_y} \varepsilon_T \tag{45}$$

ε_T is the longitudinal total strain due to the stress σ_a in the matrix far outside of the pile up, also equal to ε.

On the other hand for $D_y \ll a$, the expression for $\bar{\varepsilon}_p$ reduces to:

$$\bar{\varepsilon}_p = \varepsilon_T$$

The simple interpolation function which can satisfy the extremum of $\bar{\varepsilon}_p$ is given by:

$$\bar{\varepsilon}_p = \varepsilon_T \left[1 - \exp -\left(\frac{\Pi}{4} \frac{a}{D_y}\right) \right] \tag{46}$$

Neumann *et al.*[34] gave an expression for the derived matrix stress σ_m'', which is given by:

$$\sigma_m''(\varepsilon_T, a) = E_{matrix} [\varepsilon_T - \bar{\varepsilon}_p(\sigma_m'', \frac{a}{D_y})] \qquad (47)$$

where $\bar{\varepsilon}_p(\sigma_m'', \frac{a}{D_y})$ is the interpolation function given earlier.

On substituting the interpolation function for ε_p in the expression for σ_m'', it can be written:

$$\sigma_m''(\varepsilon_T, a) = E_{matrix} \quad \varepsilon_T \{1 - [1-\exp(-\frac{\Pi}{4} \frac{a}{D_y})]\} \qquad (48)$$

On differentiating this expression the following expression can be written:

$$\frac{d\sigma_m''}{d\varepsilon_T} = E_{matrix} \{1 - [1 - \exp(-\frac{\Pi}{4} \frac{a}{D_y})]\} \qquad (49)$$

In this expression 'a' may be geometrically related[51] to the fibre diameter $\emptyset$ by:

$$a = \emptyset(\sqrt{(\frac{\Pi}{2\sqrt{3} V_f})} - 1) \qquad (50)$$

assuming a hexagonal fibre arrangement. $\frac{d\sigma_m''}{d\varepsilon_T}$ gives the slope of the derived stress-strain curve in the second stage. The expression for $\frac{d\sigma_m''}{d\varepsilon_T}$ gives an analytical expression with D_y as the only adjustable parameter.

Neumann et al. found a 9% error in the interpolation function given for $\bar{\varepsilon}_p$. After a slight modification of this interpolation function on the basis of numerical computation, the error was estimated to be 3%. Using the modified interpolation function he calculated the value of $\frac{d\sigma_m''}{d\varepsilon_T}$ for different values of D_y to obtain agreement with the experimental values of Kelly et al.[11] $D_y = 10\mu$ is found to satisfy the experimental slopes obtained for tungsten-copper composites of different V_f.

In the present work the unmodified expression (49) was used to calculate the slope $\frac{d\sigma_m''}{d\varepsilon_T}$ by giving different values to D_y. It was found

that a single value of D_y could not give the experimental slopes for

different V_f of the tungsten-zinc composites. The different values of

D_y obtained for different V_f are tabulated along with the average experi-

mental values of $\frac{d\sigma_m''}{d\epsilon}$ in Table 9. The D_y values which can be calculated from

slip band spacing, require experimental confirmation.

In the present work the surfaces of the composite specimens were

not good enough for the direct measurement of slip band spacing. The sur-

faces could not be improved by any sort of increased polishing because

this exposed the fibres on the surface of the composite.

It should be noted that the predicted values of D_y may be

higher than the actual value. The hardening of the matrix is caused by

two phenomena taking place in the matrix:

(a) hardening due to difference in lateral

constraints of the constitutents;

(b) hardening due to dislocation pile ups.

F. Resolved Shear Stress-Strain Curves of the Composites:

These are given only to show that stress-strain curves of the

composites can be represented in the form of resolved shear stress-shear

strain curves.

C.R.S.S. varies linearly above and below V_f crit. (found theore-

tically).

The slope of the elastic-plastic region is found to vary linearly

with V_f.

TABLE 9

D_y VALUES OBTAINED FOR W-Zn COMPOSITES
ACCORDING TO NEUMANN *et al.*

AVERAGE $V_f\%$	AVERAGE $\dfrac{d\sigma_m''}{d\epsilon}$ EXP. gms/mm^2	D_y VALUES MICRONS
0.020	1.3×10^4	260
0.0365	1.6×10^4	196
0.079	2.3×10^4	141
0.312	4.1×10^4	76
0.566	1.4×10^5	71
1.130	3.4×10^5	62
2.320	3.8×10^5	42
4.580	4.3×10^5	29

V. SUMMARY AND CONCLUSIONS

1. W-Zn composites show four stages of tensile deformation.

2. In stage I, since no precise measurement of the strain was possible, the "rule of mixtures" prediction was assumed to be true for calculating strain.

3. The experimental values of the slope of stage II were appreciably higher than predicted values. The discrepancy was attributed to matrix hardening by:

      (a) different lateral constraints of the fibre and the matrix;

      (b) dislocation pile ups in the matrix near the fibres.

4. The experimental values of the ultimate tensile strength of the W-Zn composites were found to be higher than the values predicted according to "rule of mixtures". This was attributed to the matrix hardening due to dislocation pile ups in the matrix at the W-Zn interface.

5. The experimental value of V_f crit. was found to be 0.825%.

VI. SUGGESTIONS FOR FUTURE WORK

Several lines of investigation can be suggested from the discussion of the present work. These include:

(a) Further development of the experimental technique to obtain good surfaces of W-Zn composites for the measurement of the slip band spacings in the matrix.

(b) Observations on the existence of dislocation pile ups using an etch pit technique.

(c) A study of the deformation characteristics of W-Zn composites containing greater than 4.5 volume per cent tungsten fibres.

BIBLIOGRAPHY

1.   Kelly, A., Davies, G. J., Met. Rev. *10*, 1, (1965).

2.   Pattnaik, A. and Lawley, A., Met. Trans., *2*, 1529, (1971).

3.   deSilva, A.R.T. and Chadwick., Metal Science Jour., *3*, 168, (1969).

4.   Salkind, M.,George, F., and Tice, W., Trans. AIME, *245*, 2339, (1969).

5.   Alexander, J. A., Metals Engineering Quarterly., *10*, (2), *22*, (1970).

6.   Alexander, J. A., Shaver, R. G., and Withers, J. C., Review work under contract No. NASW-1779 by General Technologies Corporation for NASA.   June 1969.

7.   Morris, A. W. H., and Steigerwald, E. A., Trans. AIME, *239*, 730,(1967).

8.   Battacharyya, S., and Parikh, N. M., Met. Trans., *1*, 1437, (1970).

9.   McDanels, D. L., Jech, R. W., and Weaton, J. W., Trans. AIME, 233, 636, (1965).

10.   Kelly, A., and Tyson, W. R., Jour. Mech. and Phys. of Solids, *13*, 329, (1965).

11.   Kelly, A., and Lilholt, H., Phil. Mag., *20*, 311, (1969).

12.   Pinnel, M. R., and Lawley, A., Met. Trans., *1*, 1337, (1970).

13.   Jackson, P. W., and Cratchley, D., Jour. Mech. & Phys.of Solids, *14*, 49, (1966).

14.   Baker, A. A., Jour. of Mat. Sc., *3*, 412, (1968).

15.   Cratchley, D., Powder Met., *11*, 59, (1963).

16.   Howard, G. L., Master's Thesis, Dept. of Met., University of British Columbia, March, (1964).

17. Ahmad, I., and Barranco, J. M., Met. Trans., *1*, 989, (1970).

18. Jackson, P. W., Baker, A. A., and Braddick, D. M., Jour. of Mat. Sc., *6*, 427, (1971).

19. Cheskis, H. P., and Heckel, R. W., Met. Trans., *1*, 1931, (1970).

20. Braddick, D. M., Jackson, P. W., and Walker, P. J., Jour. of Mat. Sc., *6*, 419, (1971).

21. Stapley, A. J., Beevers, C. J., Jour. of Mat. Sc., *4*, 65, (1969).

22. Parratt, N. J., Powder Met., *7*, (14), 152, (1964).

23. Baker, A. A., Jour. of Mat. Sc., *3*, 412, (1968).

24. Whitehurst, H. B., Michener, J. W., and Lockwood, P. A., "Investigations of Glass-metal Composites," Proc. 6th Sagamore Ordnance Materials Research Conference, "Composite materials and composite structures," (AD 161443), 56, (1959).

25. Tressler, R. E., and Moore, T. L., Metals Eng. Quart. *11*, (1), 16, (1971).

26. Walton, J. D. Jr., and Poulos, N. E., Amer. Ceram. Soc. Bull., *41*, (11), 778, (1962).

27. Tyson, W. R., Davies, G. J., Brit. Jour. Appl. Phys., *16*, 199, (1965).

28. Outwater, J. O., Modern Plastics, *33*, 156, (1956).

29. Harris, B., Beaumont, P. W. R., Moncunill de Feran, E., Jour. of Mat. Sc., *6*, 238, (1971).

30. Hill, R., Jour. of Mech. and Phys. of Solids, *12*, 199 and 213, (1964).

31. Piehler, H. R., Trans. AIME, *233*, 12, (1965).

32. Cooper, G. A., Jour. of Mech. and Phys. of Solids, *14*, 103, (1966).

33. Tanaka, K., and Mori, T., Acta Met., *18*, 931, (1970).

34. Neumann, P., and Haasen, P., Phil. Mag., *23*, 285, (1971).

35. Roper, M. E., Anti corrosion, *17*, (10), 29, (1970).

36. Risebrough, N. R., Ph.D. Thesis, Dept. of Met., University of British Columbia, 5, Dec. (1965).

37. Petrasek, D. W., and Weeton, J. W., Trans. AIME, *230*, 977, (1964).

38. Max Hansen, "Constitution of Binary Alloys," Metallurgy and Metallurgical Engineering Series, 2nd Edition, McGraw-Hill Book Co., 1254, (1958).

39. Lowrie, R., and Gonas, A. M., Jour. of Appl. Phys., *36*, 2189, (1965).

40. Schmid, E., Boas, W., "Plasticity of Crystals," Chapman and Hill Ltd., 17, (1950).

41. Wert, C. A., and Tyndall, E. P. T., Jour. of Appl. Phys., *20*, 587, (1949).

42. Kelly, A., and Nicholson, R. B., Prog. Metal Phys., *10*, 151, (1963).

43. Schmid, E., Boas, W., "Plasticity of Crystals," Chapman and Hill Ltd., 59 and 123, (1950).

44. Vennett, R. M., Wolf, S. M., and Levitt, A. P., Met. Trans., *1*, 1569, (1970).

45. Tanaka, K., and Mori, T., Phil. Mag., *23*, 737, (1971).

46. Hill, R., Jour. of Mech. and Phys. of Solids, *11*, 357, (1963).

47. Love, A. E. H., "A Treatise on the Mathematical Theory of Elasticity," 4th edition, (New York Publication), 144, (1944).

48. Stuhrke, W. F., "Metal Matrix Composites," Baltimore: American Society for Testing Materials, 108, (1968).

49. Read, W. T., Phys. Rev., *78*, 275, (1950).

50. Leibfried, G., Zeit. Phys., *130*, 214, (1951).

51. Sendeckyj, G. P., Jour. of Comp. Mat., *4*, 500, (1970).